Inelastic pion scattering from ^{12}C

W. B. Cottingame*
The University of Texas at Austin, Austin, Texas 78712
and New Mexico State University, Las Cruces, New Mexico 88003

K. G. Boyer,* W. J. Braithwaite, S. J. Greene,* C. J. Harvey,† R. J. Joseph,*
D. B. Holtkamp,* and C. Fred Moore
The University of Texas at Austin, Austin, Texas 78712

J. J. Kraushaar, R. J. Peterson, R. A. Ristinen, J. R. Shepard, and G. R. Smith‡
The University of Colorado, Boulder, Colorado 80309

R. L. Boudrie, N. S. P. King, C. L. Morris, J. Piffaretti,§ and H. A. Thiessen
Los Alamos National Laboratory, Los Alamos, New Mexico 87545
(Received 19 May 1986)

Differential cross sections for inelastic pion scattering from ^{12}C at incident energies of 100 to 291 MeV and momentum transfers ≤ 300 MeV/c have been measured and are compared to results obtained from other probes, particularly electrons and protons. Angular distributions and excitation functions are presented for many of the bound states, including the 4.44-MeV (2^+,0), 7.66-MeV (0^+,0), 9.64-MeV (3^-,0), 12.71-MeV/15.11-Mev (1^+;0,1) doublet, 16.11-MeV (2^+,1), 19-MeV (4^-;0,1) doublet, and 2^- states at 18.25 and 19.4 MeV. Distorted-wave impulse-approximation calculations using both macroscopic and microscopic descriptions of the nuclear wave functions are compared to the data. The observation of an anomalous excitation function for the 15.11-MeV level and the observation of dramatic π^+/π^- asymmetries near 18 and 19 MeV excitation due to isospin mixing between 2^- states and between members of the 4^- doublet are of particular interest.

I. INTRODUCTION

Pion-induced inelastic scattering from the target nucleus ^{12}C has been extensively examined with the Energetic Pion Channel and Spectrometer (EPICS) at the Clinton B. Anderson Meson Physics Facility (LAMPF). These data include precise measurements of π^+ and π^- scattering to states below or slightly above the single-particle separation energy, i.e., ≤ 20 MeV in excitation. Angular distributions have been measured for momentum transfers out to 300 MeV/c, a range sufficient to include the first maximum for all transitions which have been observed in ^{12}C. Since these data were measured at incident pion energies of 100–291 MeV in 20- to 30-MeV increments, these data provide a unique opportunity to compare the energy dependences of natural- and unnatural-parity and isoscalar and isovector transitions with those theoretically predicted. For example, the energy dependences for transitions to natural- and unnatural-parity states are observed to differ,[1,2] and this difference has been attributed to the spin properties of the pion-nucleon interaction[3] in an impulse-approximation description of the pion-nuclear interaction. The availability of both π^+ and π^- data is an important advantage because of the sensitivity of pion inelastic scattering to isospin mixing between analog levels, as demonstrated for the 4^- doublet at $\simeq 19$ MeV (Refs. 4 and 5) and the 1^+ doublet at 12.71 and 15.11 MeV.[6]

The purpose of this paper is to present the extensive ^{12}C pion inelastic scattering data and to examine their systematic features. The pion-nuclear interaction is investigated within the context of the impulse approximation for the several different classes of transitions through comparison with results from other probes, particularly electrons and protons. Emphasis is placed on comparison of the predicted energy dependencies for the various components of the pion-nuclear interaction to those observed for transitions which can couple (in some cases exclusively) to those components. We thereby hope to isolate the interaction from nuclear-structure issues. Although it is possible to obtain agreement between impulse-approximation calculations and the ^{12}C data over certain ranges of energy for some transitions by ignoring kinematic details of the pion-nuclear interaction, we find that more consistent results can be obtained for all classes of transitions by first using pion elastic-scattering data to calibrate the energy dependence of the pion-nuclear interaction. For this reason, we first include an analysis of the elastic scattering data for ^{12}C and a discussion of the anticipated effect upon inelastic-scattering kinematics.

In Sec. II we describe the data acquisition and consider systematic errors associated with the data. In Sec. III we compare pion elastic scattering from ^{12}C to optical-model calculations to consider an appropriate treatment of kinematics in the impulse approximation. In Sec. IV we present results for pion inelastic scattering to the collective 2^+, 0^+, and 3^- states between the incident pion energies of 100–291 MeV as compared with collective model predictions. In Sec. V we give results for the isoscalar and

 ©1987 The American Physical Society

isovector 4^- and 1^+ spin-flip transitions and the isovector 2^+ natural-parity transition in comparison with microscopic calculations. Additionally we give the results for 2^- states at 18.25 and 19.4 MeV. The effects of isospin mixing and possible $\Delta_{3/2,3/2}$-hole components upon these results are considered. In Appendix I, available from the Physics Auxiliary Publication Service,[7] we examine a phenomenological model to resolve the kinematic ambiguities of the usual reduction of the first-order impulse approximation to the optical potential. In Appendix II, we examine how this model, fully constrained by elastic-scattering results, impacts the inelastic-transition amplitudes.

Tables of measured cross sections used in this work are available, and may be obtained from the Physics Auxiliary Publication Service.[7]

II. DATA ACQUISITION AND REDUCTION

EPICS consists of a pion channel which provides a momentum-dispersed π^+ or π^- beam of 50–300 MeV, a scattering chamber, and a high-resolution magnetic spectrometer for analyzing the reaction products whose momenta are ≤ 700 MeV/c.[8,9] Position-sensitive, delay-line readout drift chambers[10–12] are used to measure particle trajectories before and after the spectrometer dipoles. Computer software then uses this information to project the particle trajectories back to the scattering target and determine the incident pion momentum, scattering angle, and the momenta of the scattered particles.[13–15] The reaction kinematics are then reconstructed and the Q value is histogrammed.

With the slits fully open, the EPICS channel has a maximum momentum bite of $\pm 1\%$ of the central momentum and an intensity of 10^8 π^+/s or 2×10^7 π^-/s at energies above 160 MeV with 500 μA of primary proton beam current. The intensity is reduced by about a factor of 2 for π^+ and a factor of 1.5 for π^- at 100 MeV. With the slits fully open, 95% of the beam at the target plane is within a region extending 6.4 cm horizontally and 20.4 cm vertically and has an angular divergence of 10 mr full width at half maximum (FWHM) in the horizontal plane and 120 mr FWHM in the vertical plane. Since computer analysis should be limited to the order of 50 events/s to maintain acceptable live time, the channel momentum bite was decreased at forward scattering angles to reduce the incident pion flux. For these data, the full spectrometer momentum acceptance of $\pm 6\%$ and angular acceptance of 10 msr were used. A scattering angle acceptance of $\pm 2°$ was used for all the inelastic data.

Since these data were taken over an extended period of time, improvements in the apparatus and analysis have resulted in variations of the resolution and background. The earliest data typically had a resolution of 250–300 keV, while the resolution was 150–200 keV for the more recent data. The improvement in resolution was primarily due to vacuum coupling of the spectrometer to the target chamber. Installation of a muon rejector in the spectrometer focal plane has led to a reduction in the muon background by about a factor of 5 over the course of these measurements.

The beam intensity was monitored by an ion chamber downstream from the target. The ion chamber was preceded by an absorber of sufficient thickness to remove protons contaminating the π^+ beam. Absolute normalization of the product of the beam flux and spectrometer solid angle was accomplished by comparison of yields from elastic scattering from hydrogen with the predictions of an energy-dependent analysis of Dodder.[16] These results agree within 1–3 % with the data of Bussey.[17] The ratios of experimental yields to the predicted $\pi^+ + p$ cross sections were flat within $\pm 2\%$ between 40° and 120°. The performance of the downstream ion chamber could be monitored by comparison to an ion chamber located at the pion production target and by comparison to the integration of the primary beam current by a toroid ahead of the production target. The analysis of the data includes correction for the pion survival fraction through the spectrometer, chamber efficiency, computer live time, and the spectrometer focal plane acceptance function. The beam flux was normalized at each slit opening and each energy for both π^+ and π^-. Additionally, the cross sections for the 4.44- and 9.64-MeV levels were remeasured for a forward and a back angle point at each energy as the last phase of these measurements.

Natural carbon targets of 100- and 227-(mg/cm^2) areal densities with dimensions of 15×22 cm were used throughout. $(CH_2)_n$ (polyethylene) targets with the same dimensions as the carbon targets were used for normalization. Spectra at angles near the maxima of the angular distributions for the 1^+, 2^+, 3^-, and 4^- transitions are shown in Fig. 1. The accuracy and linearity of the EPICS system have been calibrated using the positions of known states. The uncertainty in the determination of the energy loss was found to be equal to or less than the uncertainty in determining the peak position, about 50 keV.

Yields for inelastic states were extracted from the Q-value spectra by the line-shape fitting code LOAF.[18] An instrumental line shape was first determined from an intrinsically narrow state, then line shapes for each of the other states were obtained by convolution of the instrumental line shape with a Lorentzian shape of the appropriate width. The background was simultaneously fitted with a polynomial of order up to eight. The separations between peaks were constrained to be in agreement with the known energy level assignments for ^{12}C,[19] thereby facilitating separation of overlapping states and establishing upper limits for states which were not easily observed.

Systematic errors are estimated as follows: (1) Normalization errors and flux monitoring variations are estimated at $\pm 8\%$. (2) Errors associated with corrections to the data, i.e., corrections for focal plane acceptance, efficiencies, and survival fraction, are normally less than $\pm 5\%$. However, for a position on the focal plane where the acceptance is rapidly varying the error can be large ($\pm 15\%$). (3) Extraction of yields from the background in Q-value spectra led to systematic errors for weak or overlapping states. For the low lying 2^+, 0^+, and 3^- states the systematic errors are no more than $\pm 2\%$, but for weak states such as the 15.11-MeV (1^+, $T=1$) level the systematic errors can be quite large. The overall sys-

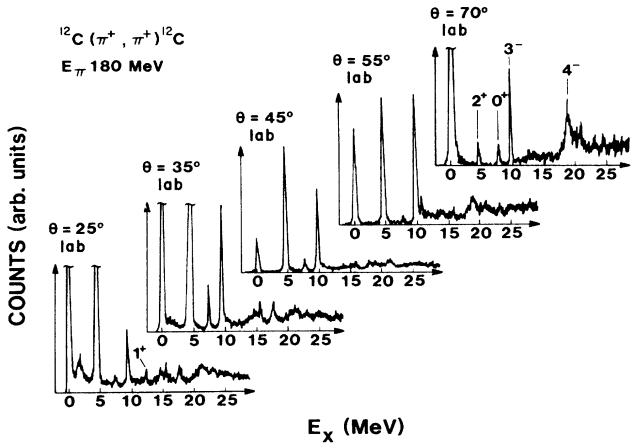

FIG. 1. Inelastic scattering Q-value spectra for π^+-^{12}C at $T_\pi = 180$ MeV and $\theta_{lab} = 25°$, 35°, 45°, 55°, and 70°.

tematic error is then estimated to be ±10%. For those points where the instrumental errors were known to be larger than normal, the statistical error bars were correspondingly increased. Systematic errors for the weakly excited states will be stated separately when required. Owing to the increased rates and increased difficulty in normalization, the forward angles ($\leq 25°$) have an uncertainty which systematically increases with decreasing angle. The overall systematic error at 15° is estimated at ±15%. The angular uncertainty is estimated to be no more than ±0.5°.

III. ELASTIC SCATTERING

In spite of the ample pion elastic scattering data extending up to 340 MeV incident energy and extending back to 120°, there remains considerable diversity among the theories which attempt to explain these data. Not only do questions remain as to kinematics,[20–22] the reaction mechanism,[23–25] the choice of form factor,[26–28] and the importance of second-order effects,[21] but diverse conceptual models yield similar comparisons to the elastic data, particularly in the region of the $\Delta_{3/2,3/2}$ resonance. Figure 2 shows a comparison of calculations for various models to the 164 MeV $\pi^+ + {}^{12}$C elastic data of Piffaretti *et al.*[29] The agreement with the data is comparable for most models within the forward hemisphere. For this reason we chose to use a model employing no more complications than are necessary to predict pion elastic scattering at angles forward of 100° in the energy region of the $\Delta_{3/2,3/2}$ resonance.

A simple systematic relationship exists between the free pion-nucleon (π-N) amplitudes and the optical-model parameters which can be used to obtain reasonable agreement between a first-order, zero-range, impulse-approximation calculation and pion elastic elastic-scattering data. Figure 3 compares the values for the optical-model parameter, b_1, predicted from the free π-N amplitudes using the frozen-target approximation, to the values obtained from a search on b_1 for the available ^{12}C data in the energy range 100–300 MeV. Both the real

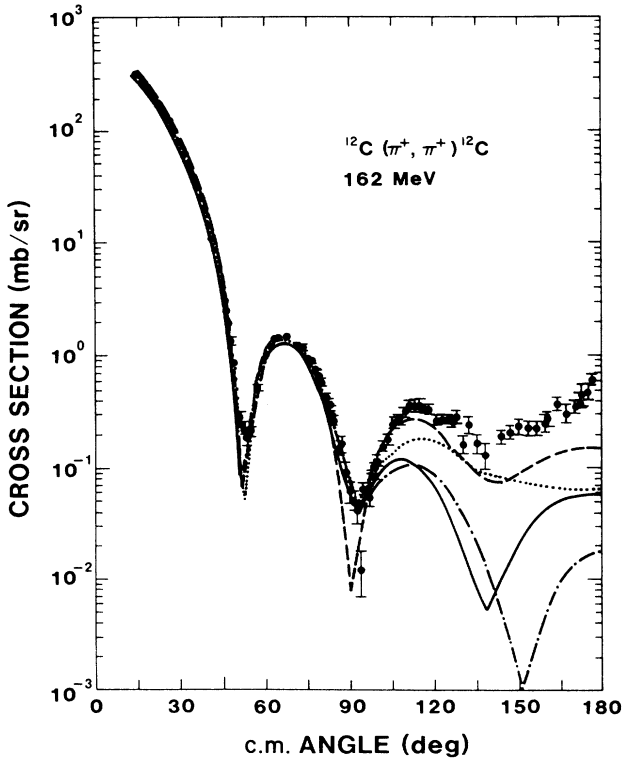

FIG. 2. Comparison of differential cross sections for various models to the 162 MeV data of Ref. 29. The solid curve is the result of our calculation. The dotted curve is the result of a first-order calculation of Chen (Ref. 88) which attempts to explain large-angle pion scattering in terms of a finite multiple-scattering series obtained from a reduction of the Watson series. The dashed curve is the result of a full potential fit (Ref. 89) using the Stricker, McManus, and Carr (Ref. 64) representation for the optical potential. The dotted-dashed curve shows the results of an isobar-doorway model calculation of Horikawa, Thies, and Lenz (Ref. 90).

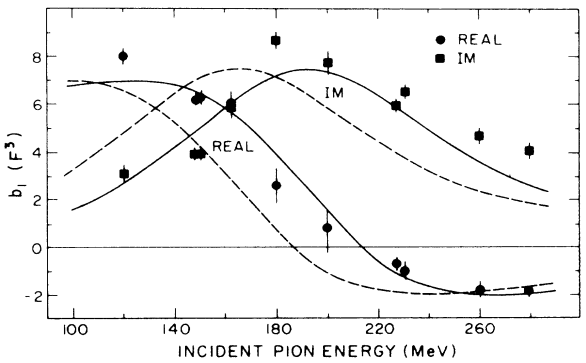

FIG. 3. Real and imaginary values for the optical-model parameter b_1. The points are the result of a search on b_1 for the ^{12}C data shown in Fig. 4. The dashed lines are the real and imaginary values for b_1 predicted from the free π-N amplitudes using a frozen-target approximation. The solid curves are the real and imaginary values for b_1 assuming a −28-MeV shift in energy at which the optical-model parameters were calculated.

and imaginary parts of b_1 obtained from the search exhibit a rather uniform shift in energy from their predicted values. It is only the strong energy dependence of the $\Delta_{3/2,3/2}$ resonance which makes this shift significant. The solid curve of Fig. 4 shows calculated differential cross sections for ^{12}C with a -28 MeV shift in the energy at which the optical-model parameters were calculated. The dashed curve represents the same calculations without the kinematic shift. The obvious effect is that this single phenomenological parameter gives an energy dependence which is in better agreement with the data. The predictions for the total cross section for the same calculations are compared to the ^{12}C data in Fig. 5. Similar results for nuclei ranging from ^{9}Be to ^{208}Pb have been observed and are reported in Ref. 30. In all cases the kinematic energy shift is about -30 MeV for incident pion energies of 100–300 MeV.

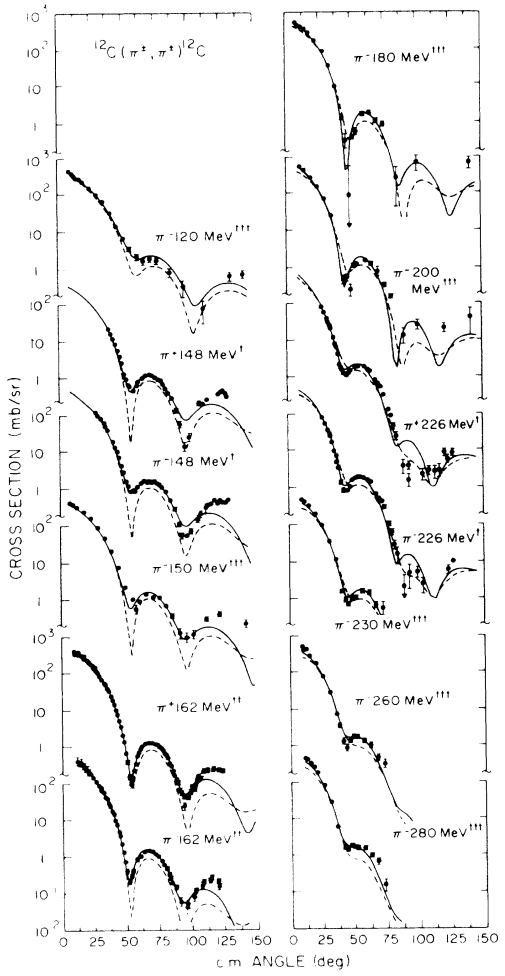

FIG. 4. Differential cross sections for pion-induced elastic scattering for ^{12}C data in the region of 100–300 MeV. The dashed curve represents frozen-target calculations and the solid curve includes a -28-MeV shift in the energy at which the optical model parameters are calculated. These data are from Refs. 47†††, 29†, and 91.††. [Daggers (†, ††, or †††) denote the sources of the data plotted, i.e., in this figure, π^-, 120 MeV is from Ref. 47, etc.]

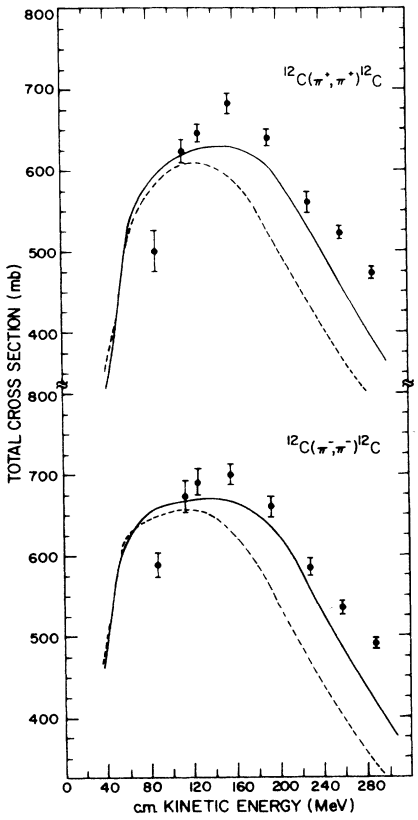

FIG. 5. Total cross sections for pion scattering from ^{12}C. The dashed curve represents frozen-target calculations and the solid curve includes a -28-MeV shift in the energy at which the optical-model parameters were calculated. These data were from Ref. 92.

Justification for the use of this phenomenological kinematic shift in energy becomes apparent upon examination of the usual reduction of the first-order impulse approximation. The collision energy [the energy available to the π-N two-body system in the pion-nuclear (π-A) c.m.] used in these reductions are ambiguous since no relativistic, invariant many-body theory exists. Appendix I, available from the Physics Auxilary Publication Service,[7] demonstrates that the Fermi motion of the target nucleons can give rise to a reduction in the collision energy similar to that used in the previous calculations.

The coordinate-space optical-model computer code, PIRK,[31] with the modifications described in Appendix I, is used to solve a Klein-Gordon equation containing only linear terms in the optical potential. A Kisslinger form[24] for the optical potential is assumed,

$$\langle \kappa' \mid t(\omega(\kappa)) \mid \kappa \rangle = a_0 + a_1 \kappa' \cdot \kappa \ , \tag{1}$$

where κ and κ' are the "effective on-shell momenta" described in Appendix I, $t(\omega(\kappa))$ is the t-matrix containing the π-N collision energy, $\omega(\kappa)=\omega_\pi(\kappa)+\omega_n(\kappa)$, and a_0 and a_1 are related to the π-N amplitudes given in Eq. (A4). The coordinate-space representation for the solution

of the nuclear part of the Klein-Gordon equation is[32]

$$\langle \mathbf{r} \mid U_{\mathrm{KG}} \rangle = -\{b_0\kappa^2\rho(r)+b_1\nabla_r\cdot[\rho(r)\nabla_r]\} , \quad (2a)$$

$$b_0 = -2(2\pi)^3\omega_\pi(\kappa)a_0/\kappa^2 , \quad (2b)$$

$$b_1 = -2(2\pi)^3\omega_\pi(\kappa)a_1 . \quad (2c)$$

The optical-model parameters, b_0 and b_1, are evaluated using Eq. (A4),

$$b_l = \frac{4\pi}{\kappa^3}\frac{\kappa\omega_{\mathrm{N}}^*(\kappa^*)}{\kappa^*\omega_{\mathrm{N}}(\kappa/A)}(\kappa^* f_l^*) . \quad (3)$$

The superscripted asterisk denotes variables in the π-N c.m. It should be made clear that the energy-shifted kinematics of Appendix I is only used for determination of the optical-model parameters, b_0 and b_1, and the momentum term, κ^2, in Eq. (2).

For all of these calculations, both elastic and inelastic, the amplitudes, f_l^*, are constructed from the π-N phase shifts of Rowe, Salomon, and Landau,[33] and the density distribution, $\rho(r)$, for ^{12}C is obtained from a modified harmonic-oscillator density distribution with parameters taken from electron-scattering results,[34,35]

$$\rho(r)=\rho_0(1+c(r/a)^2)\exp[-(r/a)^2] ,$$

$$\rho_0=[(1+\tfrac{3}{2}c)(\sqrt{\pi}a)^3]^{-1} , \quad (4a)$$

$$a=1.514 \text{ fm}, \quad c=1.674 . \quad (4b)$$

The electron-scattering parameters given in Eq. (4b) have been modified to remove the finite charge size of the proton to obtain a point-density distribution consistent with our on-shell assumptions. For ^{12}C the modified harmonic-oscillator model gives a density distribution which is within the error envelope of model-independent results which are well determined out to 4.5 fm or about 1% of the central density.[36] This density distribution is shown in Fig. 6.

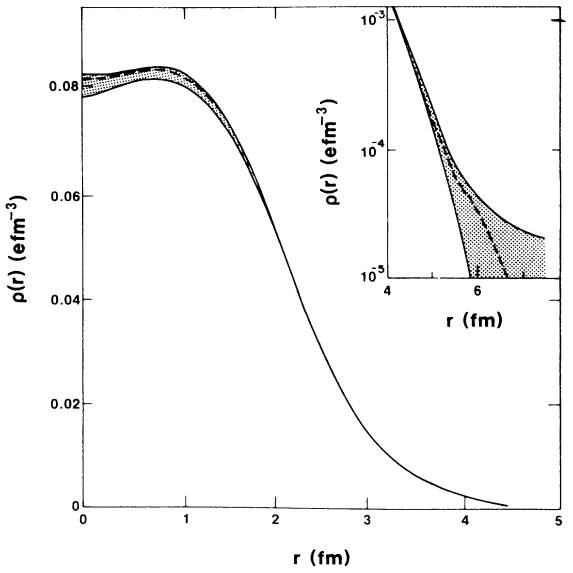

FIG. 6. Density distribution for ^{12}C. The solid lines define the error envelope of model-independent analysis of both high and low q electron scattering data (Ref. 36). The dashed curve is the electron-scattering, modified-harmonic-oscillator density distribution (Ref. 35).

To predict pion elastic scattering data in the resonance region forward of 100°, it is only necessary for a model to determine the peripheral partial-wave amplitudes due to the nuclear "blackness."[37] Our analysis indicates that these partial waves, $5 \leq l \leq 7$ for ^{12}C at 164 MeV, are critical for the angular region 30°–100°. Therefore, any model which accurately determines amplitudes for these partial waves will be successful in this region. However, to produce the larger, backward-hemisphere cross sections as indicated by the 164 MeV ^{12}C data[29] requires dramatically adjusting the real part of the lower partial-wave amplitudes by second order effects.[38] None of the existing theories predict such values for the lowest partial waves, and therefore we do not consider the large-angle data.

The conspicuous lack of consideration given to several aspects of pion-nuclear scattering may suggest that the agreement between data and the calculations shown in Fig. 4 and in Ref. 30 is fortuitous. However, within the region of the $\Delta_{3/2,3/2}$ resonance, the strong surface nature of the π-nucleus interaction may justify ignoring nuclear-medium effects, which at other energies may be critical. The sensitivity to the finite size of the pion-nucleon form factor and nuclear correlations are greatly reduced if the interaction is contained in a region where the local density is only a fraction of the central density. Furthermore, a pion range[39–43] of about 1 GeV/c is consistent with the assumption of an essentially on-shell interaction. Except for the $|\mathbf{q}|$ dependence which is dropped from our estimation for the collision energy, the on-shell assumptions of Eq. (A4) and the assumption that our kinematic shift has affected a correct factorization of Eq. (A3) are inconsistent with the inclusion of the standard "angle transformation." (See Ref. 22, pp. 172–174, for a discussion of this subject.) The neglect of the $|\mathbf{q}|$ dependence in the collision energy should have little effect, except at large angles, where far more sophisticated models fail.[38] The absence of corrections for pion absorption is justified if the process of absorption at resonance energies generally involves a sufficient number of interactions to have prevented the pion from returning to the entrance channel and consequently will not affect elastic scattering.[44] We conclude that the energy-shifted optical model is an adequate representation at moderate momentum transfers for the pion-^{12}C interaction near the $\Delta_{3/2,3/2}$ resonance.

IV. SPIN-INDEPENDENT TRANSITIONS

Since the low-lying states in ^{12}C are known to be collective in nature, having negligible spin-flip contribution in the transition from the ground state,[45,46] we begin by considering the 4.44-MeV $(2^+,0)$, 7.66-MeV $(0^+,0)$, and 9.64-MeV $(3^-,0)$ transitions. The present data for pion-induced inelastic scattering to these states are shown in Figs. 7–9. These data span the energy region of the $\Delta_{3/2,3/2}$ dominance and an angular range which encom-

passes the first maximum of transitions with angular momentum transfer up to 300 MeV/c. The systematic errors for these data are generally as previously estimated. However, for the early 162-MeV data, the large background increased the difficulty in extracting cross sections near 10 MeV. This is reflected in the anomalous points at forward angles and the inconsistently large cross sections in the region of the minimum and second maximum for the 3^- 162-MeV data. Figure 10 compares the present data for the 2^+ state which overlap previous 180-MeV data of Binon[47] and the 162-MeV data of Piffaretti.[29] Only in the region of the second maximum and second minimum is there disagreement. Similar discrepancies on the order of 20% are also observed between the present 162 MeV data and those of Ref. 29 for the 0^+ and 3^- levels. The 180 MeV π^+/π^- data previously reported,[48] although about 8% lower at the maximum, are within our estimate of systematic errors.

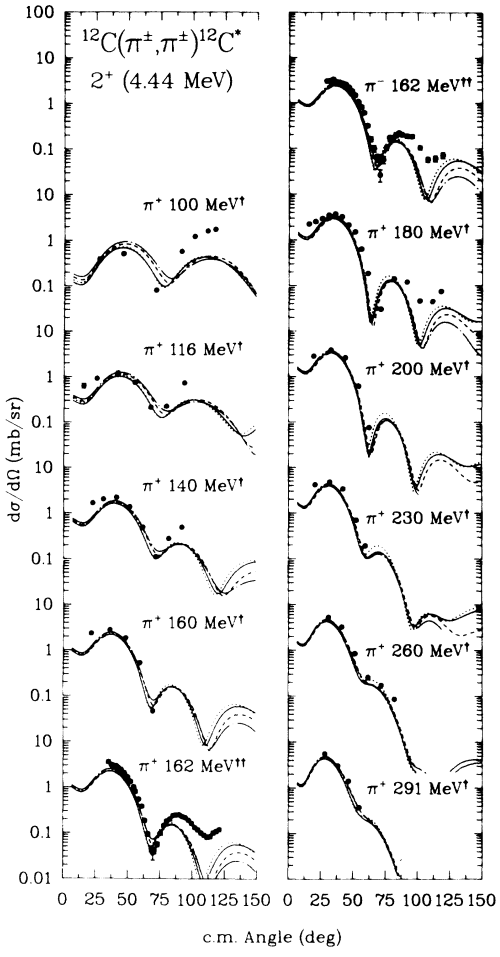

FIG. 7. Differential cross sections for pion-induced inelastic scattering to the 4.44-MeV (2^+;0) state in ^{12}C in the region of 100–300 MeV for the present data† and those of Ref. 91.†† The solid curves are results of collective model calculations assuming a 3PF ground-state density distribution. The dotted curves are from Tassie-model calculations assuming a MHO ground-state density distribution. The dashed curves represent results from calculations where the transition densities were empirically deduced from electron scattering. The dashed-dotted curves are results from calculations using microscopic descriptions of the transition densities.

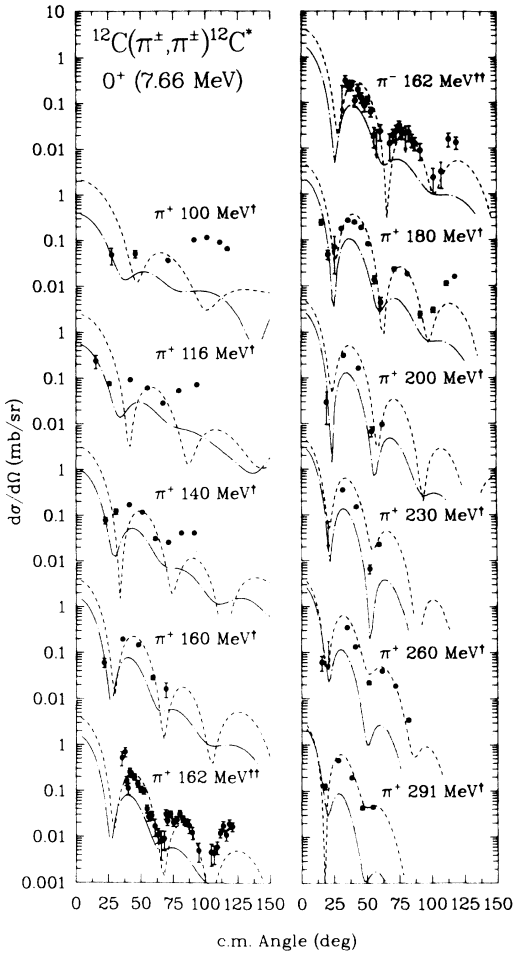

FIG. 8. Same as Fig. 7, except for the 7.66-MeV (0^+;0) state of ^{12}C.

The curves represent first-order, configuration-space, distorted-wave impulse-approximation (DWIA) calculations where the initial and the final pion distorted waves are obtained from the elastic optical potential using the methods previously discussed. The frozen-target approximation assuming on-shell kinematics with a collision energy deduced from elastic scattering is also used in the evaluation of the inelastic scattering matrix. Figure 11 compares calculations for the 2^+ (4.44-MeV) state with and without a kinematic energy shift of -28 MeV in the inelastic scattering matrix. Although not dramatic, the energy dependence at the first maximum is more accurately reproduced by the inclusion of this phenomenological energy shift. Attempts to treat the inelastic kinematic shift as a free parameter while also allowing the transition strength to vary results in values which are consistent

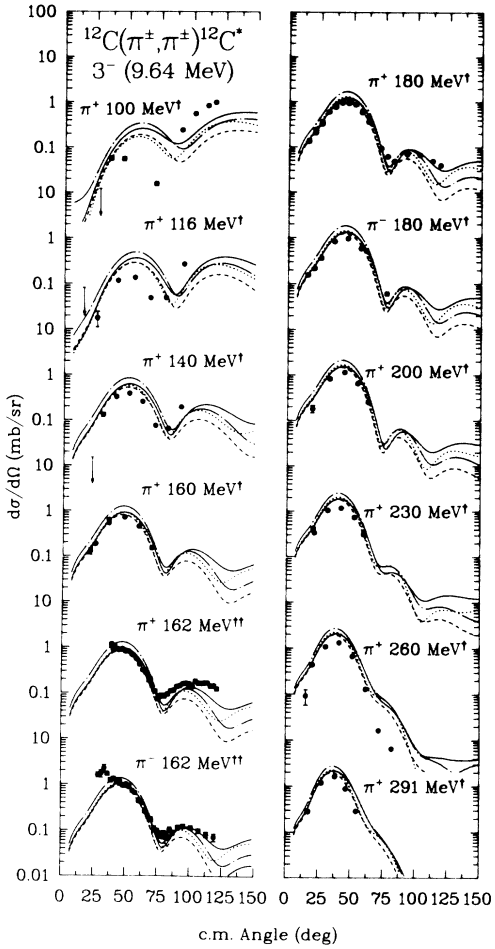

FIG. 9. Same as Fig. 7, except for the 9.64-MeV (3^-;0) state of ^{12}C.

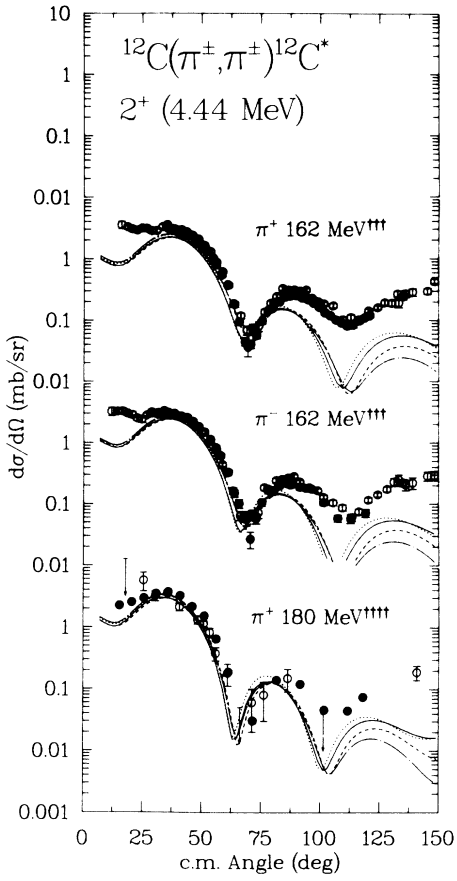

FIG. 10. Comparison of EPICS data (solid circles) with those of Refs. 29††† and 47†††† (open circles). The curves are the same as in Fig. 7.

with those previously determined for elastic scattering.

Inclusion of this phenomenological energy-shift parameter into the inelastic scattering matrix is plausible since the factorization of the inelastic t matrix, as demonstrated in Appendix II (available from the Physics Auxiliary Publication Service[7]), is entirely analogous to that for the elastic factorization. Implementation of the phenomenological energy shift into our first-order, configuration-space calculations is also described in Appendix II.

The inelastic cross sections are calculated according to Eq. (A13) using the coordinate-space DWIA computer code, UTDWPI.[49] Figures 7–11 compare the measured cross sections with the UTDWPI calculations. The solid, dashed, and dotted lines represent only the spin-isospin independent component of the transition density. The dotted-dashed curves represent microscopic calculations which will be discussed later. The solid lines are the results from a model where the transition densities are given in terms of collective nuclear excitations of angular momentum λ and projection μ,[50] i.e.,

$$\rho(\mathbf{r})=\sum_{\lambda\mu}\beta_\lambda F_\lambda(r)Y_{\lambda\mu}(\hat{\mathbf{r}})\frac{(-1)^\mu}{\hat{J}'}\langle J'M' \mid JM\lambda-\mu\rangle \ , \tag{5a}$$

$$F_\lambda(r)=c\frac{\partial}{\partial c}[\rho_{\text{g.s.}}(r,c)]\bigg|_{c=c_0} =-c\frac{\partial}{\partial r}[\rho_{\text{g.s.}}(r,c)]\bigg|_{c=c_0} \ , \tag{5b}$$

$$\rho_{\text{g.s.}}(r)=\rho_0(1+w(r/c)^2)\Big/\left[1+\exp\left[\frac{r-c}{z}\right]\right] \ . \tag{5c}$$

The notation $\hat{J}'$ implies $(2J'+1)^{1/2}$. The Clebsch-Gordan coefficient reduces to $\delta_{J\lambda}\delta_{M-\mu}$ for the 0^+ ground state of ^{12}C. The ground-state matter density distributions, $\rho_{\text{g.s.}}$ [taken to be three parameter Fermi (3PF) models with half-density radii, c_0, and diffusivity parameters, z], were obtained from electron-scattering charge distributions[35] by the deconvolution of the proton form factor. The normalization, ρ_0, is chosen such that $\int r^2dr\,\rho_{\text{g.s.}}=1$. The deformation parameter, β_λ, is related to the reduced electric transition probability, $B(C\lambda)$, and the electric transition width, $\Gamma_\lambda^{(E)}$, by,

$$B(\sigma\lambda)\downarrow=(\hat{J}/\hat{J}')^2 B_\lambda^{(\sigma)}(J\to J')$$
$$=|M_\lambda^{(\sigma)}|^2=\left|Z\int r^2dr\, r^{k(\sigma)}\rho_\lambda^{\mathrm{tr}}(r)\right|^2 ,$$
$$\rho_\lambda^{\mathrm{tr}}(r)=\beta_\lambda F_\lambda(r),\quad k(C,E)=\lambda,\quad k(M)=\lambda-1 , \tag{6a}$$

$$\Gamma_\lambda^{(\sigma)}=\frac{8\pi\alpha^{(\sigma)}(\lambda+1)}{\lambda((2\lambda+1)!!)^2}\frac{E_x^{2\lambda+1}}{(\hbar c)^{2\lambda}}B_\lambda^{(\sigma)\downarrow} ,$$
$$\alpha^{(C,E)}=\frac{e^2}{\hbar c},\quad \alpha^{(M)}=\frac{e^2}{m_p c^4} , \tag{6b}$$

for $\lambda\neq 0$. For $\lambda=0$ the reduced matrix element is defined as $M_0^{(E)}=Z\int r^4dr\,\rho_0^{\mathrm{tr}}(r)$.

The dashed curves represent hydrodynamic model calculations within the Tassie[51] formulation, for which the distorted density and deformation parameters are given by

$$F_\lambda(r)=r^{\lambda-1}\frac{\partial}{\partial r}[\rho_{\mathrm{g.s.}}(r)] ,$$
$$\beta_\lambda=\frac{M_\lambda^{(E)}}{Z\int r^{\lambda+2}dr\,F_\lambda(r)} . \tag{7}$$

Here, $\rho_{\mathrm{g.s.}}(r)$ is taken to be the modified-harmonic-oscillator (MHO) density distribution given by Eqs. (4). This MHO ground-state density is the same as used in the calculation for the elastic and the distorted waves.

The dotted curves represent matter transition densities empirically deduced from electron scattering.[45,46,52,53] The parametrization used to fit the electron-scattering form factors was that of random-phase-approximation (RPA) shell-model transition densities,

$$\rho_\lambda^{\mathrm{tr}}(r)=\rho_0 r^\lambda(1+cr^2+zr^4)\exp(-wr^2) , \tag{8a}$$
$$\rho_0=M_\lambda^{(E)}/Z\int r^{\lambda+2}dr\,r^\lambda(1+cr^2+zr^4)\exp(-wr^2) . \tag{8b}$$

These transition densities were used for comparison to proton scattering by Gustafsson and Lambert.[54] The deformation parameters extracted from proton scattering have been shown to be independent of the beam energy over a wide range.[55]

Our calculations are normalized to the electron-scattering reduced matrix elements determined from that reference. Therefore, the pion-scattering results can be compared directly to both the electron- and proton-scattering data.

Figure 12 displays the radial transition densities for the

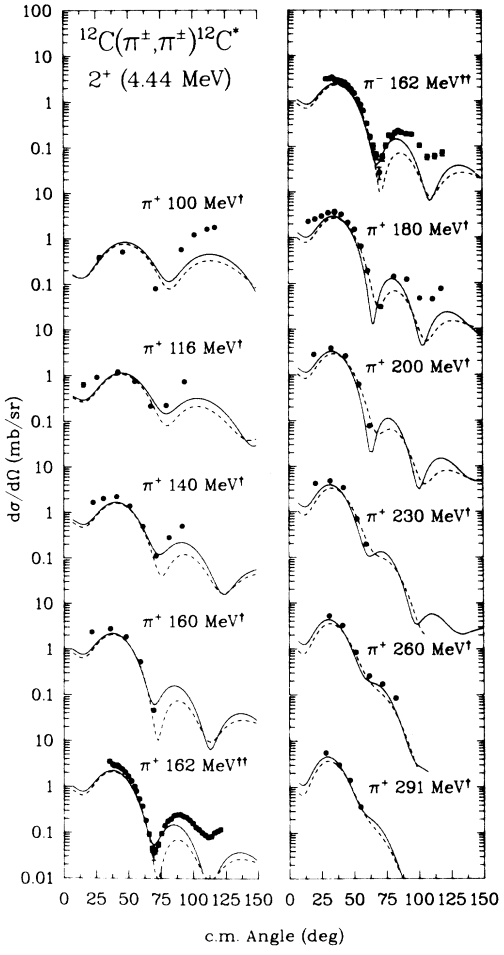

FIG. 11. Comparison of calculations with a kinematic shift of −28 MeV (solid line) and with no kinematic shift (dashed line) in the inelastic t matrix. These calculations used the collective model but the same results are obtained with either of the other models.

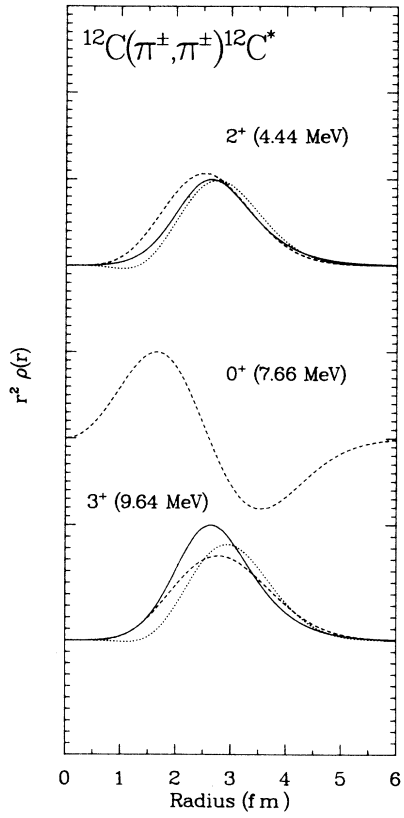

FIG. 12. Radial transition densities for the macroscopic models used in our calculations. The solid, dashed, and dotted curves are as indicated in Fig. 7.

TABLE I. Macroscopic model parameters used in calculations.

State	c	z	a	$\Gamma^{(E)a}$ (10^{-3} eV)	Model
2^+	2.355	0.5224	−0.149	11.3	Collective (3PF)
	1.649		1.762	11.3	Tassie (MHO)
	0.487	0.0	0.437	11.3	Empirical (e,e′)
0^+	0.283	0.006 32	0.321	1.74 fm[2b]	Empirical (e,e′)
3^-	2.355	0.5224	−0.149	0.220	Collective (3PF)
	1.649		1.762	0.220	Tassie (MHO)
	0.0	0.0	0.325	0.220	Empirical (e,e′)

[a]In all cases calculations were normalized to produce the quoted value for the transition width.
[b]Value for reduced matrix element, $M_\lambda^{(E)}$.

2^+, 0^+, and 3^- transitions. The transition densities for each state, which have been normalized to the same value for the reduced matrix element, are quite similar beyond the half-density point. This similarity results in similar predictions for pion scattering in the region of the $\Delta_{3/2,3/2}$ resonance. Since a collective calculation was considered inappropriate, only the empirical transition density is given for the 0^+ transition. Indeed, calculated angular distributions using either the 3PF or the MHO are out of phase with the 0^+ data at all energies. Table I gives the matter density parameters and transition widths used in each case.

The agreement between data and calculation above 140-MeV incident pion energy is good for most models within the forward hemisphere, but, in contrast to the results for elastic scattering, there is a systematic failure below 140 MeV. Additionally, coupled-channel calculations[56] indicate that the forward-angle cross sections for the 0^+ state become increasingly suppressed as the incident pion energy falls below 150 MeV if two-step processes are included. Although there is an indication in our forward-angle data that such a process may be contributing to the failure of the DWIA for the 0^+ transition at the lower energies, the most obvious deficiency is the dramatic underestimation of the cross sections at angles beyond 70° and below 140 MeV. If we ignore the data of 140 MeV and below, the data show the same trend as is observed for proton scattering.[55] The electron-scattering transition widths give cross sections which are 20–30 % low for the 2^+ transition and 15–30 % high for the 3^- transition. The cross sections for the 0^+ transition are adequately reproduced by the empirical electron-scattering transition density, considering the statistical and systematic uncertainties in the data.

By defining a sensitivity function as

$$G_L(r)\simeq\sum_{l,l'}\int d\hat{\mathbf{r}}\frac{\chi_{l'}^{-*}(r)}{r}Y_{l'm'}(\hat{\mathbf{r}})\{-b_0\kappa_n^2 Y_{LM}(\hat{r})+b_1\nabla_r\cdot[Y_{LM}(\hat{\mathbf{r}})\nabla_r]\}\frac{\chi_l^+(r)}{r}Y_{lm}(\hat{\mathbf{r}})\ , \tag{9a}$$

$$\sigma_{\text{total}}\simeq\left|\int r^2dr\,G_L(r)F_\lambda(r)\right|^2\ , \tag{9b}$$

i.e., the radial transition density is set to 1 and the angle-integrated cross section is observed as a function of the nuclear radius, the effect of the distortions and angular momentum transfer can be observed as a function of the incident pion energy. Figure 13 shows the sensitivity function for the incident pion energies of 100, 160, and 260 MeV. At energies of 160 MeV and greater, the cross sections are sensitive to nuclear regions beyond the half-density radius at 2.4 fm. However, at 100 MeV the pion has penetrated beyond the nuclear surface and is most sensitive to a radius of about 2 fm for all values of L. Since the transition densities remain large at 2 fm, the overlap between the sensitivity function and the transition density will result in a large contribution to the cross section from that region. Therefore, it may be that in the case for the 2^+, 0^+, and 3^- transitions, our simple impulse approximation is breaking down at low energies as a direct result of the pion penetrating the nuclear medium.

At least for these spin-independent inelastic transitions, the DWIA provides reasonable agreement with the data for incident pion energies above 140 MeV for properly normalized collective models or empirical electron-scattering transition densities. The phenomenological energy shift appears to be a simple method for incorporation of a correction to the frozen-target approximation as applied to the inelastic interaction for the Fermi momentum of the target. Empirically, it results in the determination of transition probabilities that are independent of energy above 140 MeV.

V. SPIN-DEPENDENT TRANSITIONS

Next, we consider transitions having large spin-flip contributions. Transitions between the 0^+ ground state and states of unnatural parity, such as the 12.71-MeV/15.11-MeV $(1^+;0,1)$ doublet and the 19-MeV $(4^-;0,1)$ doublet[57] in ^{12}C, can proceed only through the spin-dependent part of the interaction.[58] The transition to the 16.11-MeV

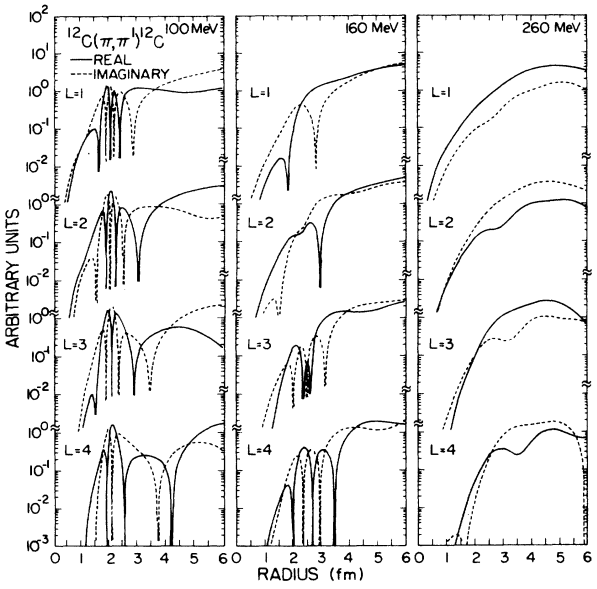

FIG. 13. Absolute value of the real (solid line) and imaginary (dashed line) parts of the sensitivity function as described in Eq. (9a) for $L=1$, 2, 3, and 4.

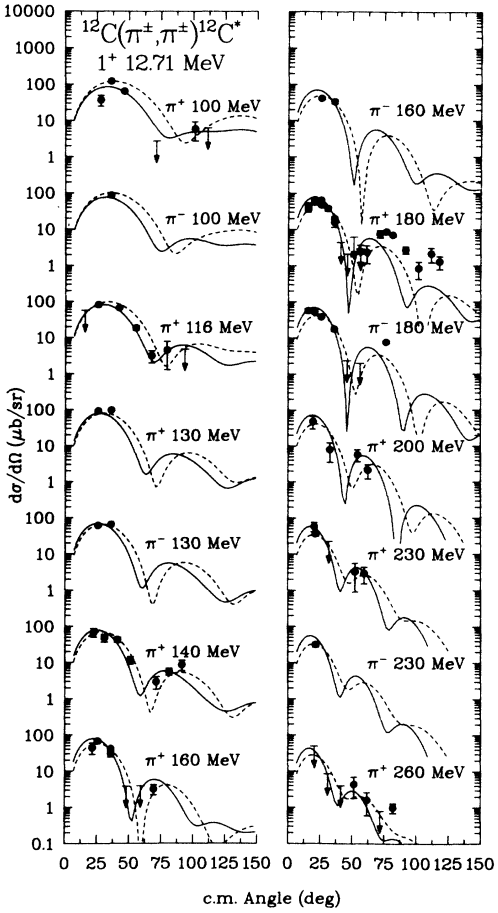

FIG. 14. Differential cross sections for pion-induced inelastic scattering to the 12.71-MeV (1^+;0) level in ^{12}C in the region of 100–300 MeV incident pion energy. The curves are results of microscopic calculations using the particle-hole spectroscopic amplitudes given in Table II. The solid (dashed) curves are the results of using the harmonic-oscillator parameter a (b).

(2^+,1) level in ^{12}C, although of natural parity, is also known to have a large spin-dependent contribution.[59] Figures 14–17 show data for inelastic scattering to the 1^+, 2^+, and 4^- levels in ^{12}C at incident pion energies from 100 to 291 MeV. For the 1^+ levels, the data are adequate to define the position and magnitude of the first maximum, but there are sufficient statistics to define the position of the first minimum or second maximum only at a few energies. The 15.11-MeV level was situated on a broad structure of about 2 MeV FWHM,[60] presumably a 2^+ $T=0$ state,[61] which leads to ambiguities in the choice for the line shape used for fitting the peak. It was determined that the yields could be altered by as much as ±15% by choosing equally plausible line shapes. Consequently, the systematic errors for cross sections beyond the first maximum can be as large as ±20%. Cross sections for the 2^+ 16.11-MeV state should be considered to have an additional systematic fitting error of 10%. These data are, in part, the result of reanalysis of the data presented in Ref. 62. Subsequent higher quality data have allowed a better determination of the background content. The 180 MeV π^+ data for the 19.25-MeV level contain a point 40% below the other data. This point, as well as that for π^- at 180 MeV, and the 19.65-MeV π^+ and π^- 180 MeV points were measured separately from the other data for the purpose of accurately determining the ratio of yields for π^+ and π^-. Although the relative uncertainty in these yields is small, $\lesssim 5\%$, the absolute normalization was not determined at 180 MeV, but was extrapolated from a lower energy. The error in this extrapolation is thought to be the source of this discrepancy.

The curves represent DWIA calculations as outlined in Appendix II, but now including the spin-dependent components which were omitted in Eq. (A12). For the spin-dependent part of the interaction we use the zero-range spin-orbit operator which Carr *et al.*[63] have demonstrated to predict the effective pion-nucleus interaction for the stretched 4^- and 6^- states in ^{16}O and ^{28}Si. The configuration-space, p-wave form of the spin-orbit operator was given by

$$t^*_{\pi N}(\mathbf{r})=(a_2+\bar{a}_2\mathbf{I}_\pi\cdot\boldsymbol{\tau}_i)\nabla_r\delta(\mathbf{r})\times\boldsymbol{\kappa}^*\cdot\boldsymbol{\sigma}_i\ , \tag{10}$$

where $\delta(\mathbf{r})=\delta(\mathbf{r}-\mathbf{r}_i)$ is the relative coordinate, $\boldsymbol{\kappa}^*$ is the pion c.m. momentum, and the strength parameters, a_2 and $\bar{a}_2$, are the same as given in Eq. (A11). Equation (10) is consistent with the spin-dependent part of the momentum-space representation contained in Eq. (A11), where the strength parameters are evaluated at the effective on-shell collision energy. Carr *et al.* found the spin-dependent component of this model to be equivalent to the Stricker, McManus, and Carr (SMC) form[64] at 162 MeV. However, as can be seen from Fig. 17, the DWIA calculations for a kinematic shift of −28 MeV (solid line) have a different energy dependence from calculations with

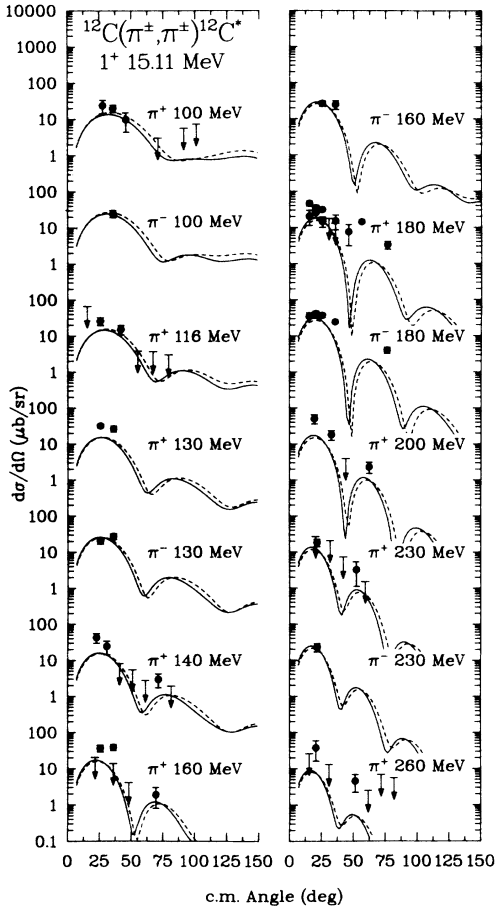

FIG. 15. Same as Fig. 14, except for the 15.11-MeV (1^+;1) level and dashed curve uses the harmonic-oscillator parameter c.

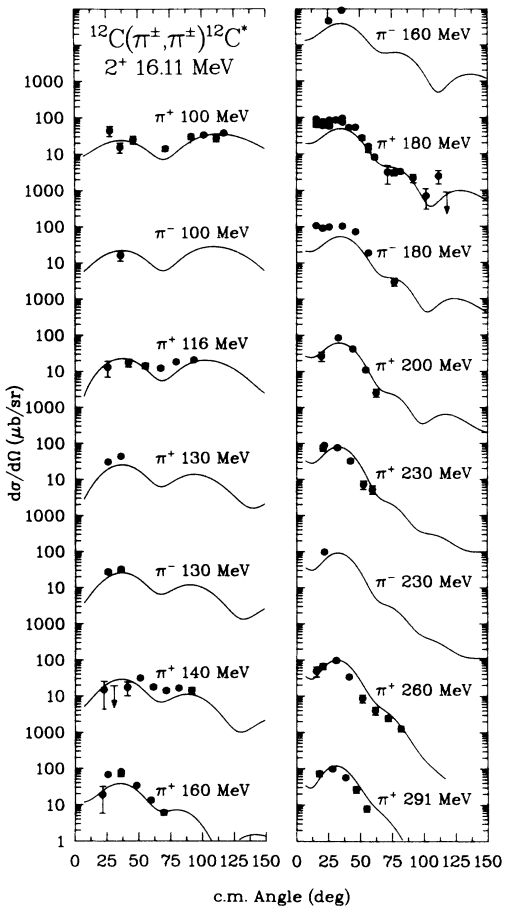

FIG. 16. Same as Fig. 14, except for the 16.11-MeV (2^+;1) level.

no kinematic shift (dashed line) for the 4^- states in ^{12}C. The two calculations differ by a factor of 2 at 291 MeV, while virtually total agreement is retained at 160 MeV. This is due, in part, to the strong energy dependence in the spin-dependent components above 160 MeV and, in part, to the diminished effects of the distortions for high-spin states.[3] These calculations were performed using a modification of the generalized inelastic scattering potential code ALLWRLD (Ref. 65) to calculate the transverse spin transition density from harmonic-oscillator wave functions given in the *j-j* coupling scheme and to form the subsequent folded potential using the interaction of Eq. (10). The pion distorted-wave code UTDWPI (Ref. 49) was used to generate the distorted potential and to form the differential cross sections.

We consider first the 4^- transitions observed in pion inelastic scattering by Moore *et al.*[1] as well as in electron scattering.[57] The stretched configuration,[66] $[1d_{5/2}\text{-}1p_{3/2}^{-1}]4^-$, of these states reduces the possible complexities to a minimum. First, in the impulse approximation, only the transverse spin transition density can contribute. Second, the corrections to the impulse approximation for Fermi motion which led to terms involving pionic current coupling to the nuclear convection current cannot contribute to stretched configurations.[3] Third, $\Delta_{3/2,3/2}$-hole admixtures which may contribute to isovector transitions (such as the 1^+ isovector transition in ^{12}C) are negligible for high-spin states.[67] However, it is still possible to have contributions from coupling of the spin-orbit component of the π-N interaction to the nuclear spin-current transition density which is not considered in these impulse-approximation calculations.

We have previously attributed the large π^+/π^- asymmetries, which can also be seen in the present data, to isospin mixing between the members of the 4^- doublet, resulting in the 19.25-MeV level being proton-like and the 19.65-MeV level being neutron-like.[4] The ratio for $\sigma_{\pi^+}/\sigma_{\pi^-}$ was originally observed to be greater than 2:1 and less than 1:2 for the 19.25-MeV state and 19.65-MeV levels, respectively.[5] Assuming $\Delta_{3/2,3/2}$ dominance and two-state mixing, the admixture amplitude of the $T=1$ component into the otherwise pure $T=0$ level at 19.25 MeV (or, conversely, of the $T=0$ component into the 19.65-MeV level), i.e.,

$$
\begin{aligned}
&|A\rangle=\alpha\,|T=0\rangle-\beta\,|T=1\rangle\ ,\\
&|B\rangle=\alpha\,|T=1\rangle+\beta\,|T=0\rangle\ ,\\
&\alpha^2+\beta^2=1\ ,
\end{aligned}
\tag{11}
$$

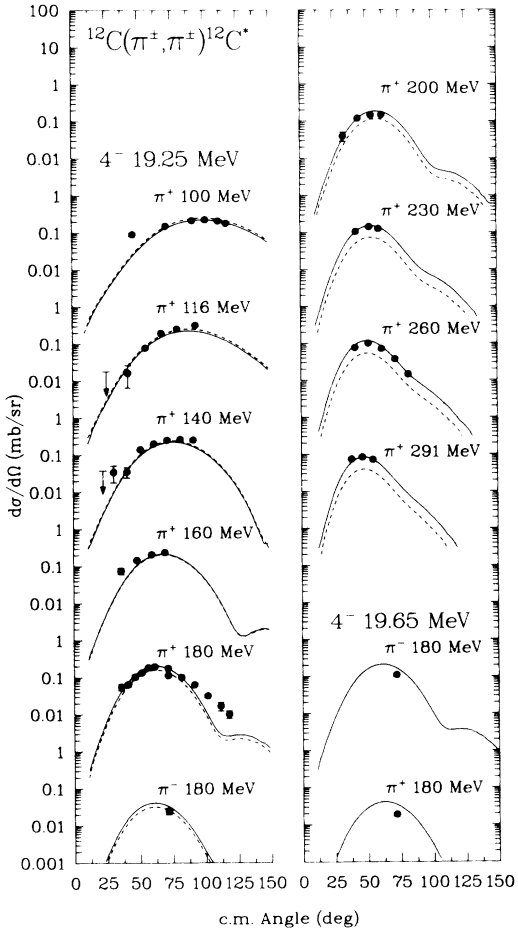

FIG. 17. Differential cross sections for pion-induced inelastic scattering to the 19.25- and 19.65-MeV levels in ^{12}C. Both curves use the oscillator parameters and spectroscopic amplitudes given in Table II, but the dashed curves do not include a kinematic shift.

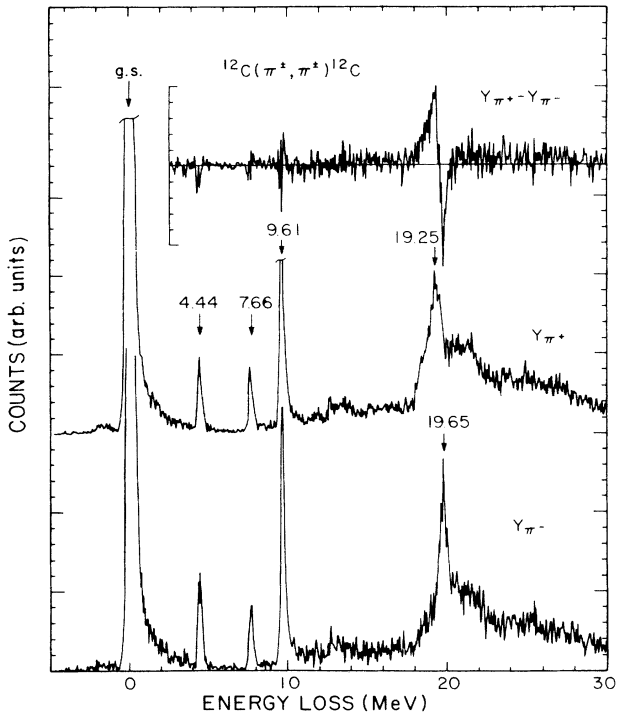

FIG. 18. Q-value spectra for π^+, π^-, and the difference for inelastic scattering at $T_\pi = 180$ MeV and $\theta_{lab} = 70°$.

was estimated to be $|\beta| \geq 0.32$. This estimate assumes that the physical separation is sufficient that β can be considered as real. Siciliano and Weiss[68] considered the effects of differences in proton and neutron wave functions at the nuclear surface upon π^+/π^- asymmetries. They concluded that such "external" Coulomb effects for states near particle threshold lead to π^- enhancements for inelastic scattering to both isovector and isoscalar states (about a factor of 2 greater π^- enhancement for the $T=1$ state than for the $T=0$ state) and *cannot* give rise to the bipolar shape observed in the difference spectra for the 4^- doublet in ^{12}C. Halderson *et al.*[69] considered the effect of the continuum upon the 4^- one-particle–one-hole stretched configuration in ^{12}C by generating the excited-state wave functions from the recoil-corrected continuum shell model (RCCSM).[70] They attribute the high isospin mixing of the 4^- states to two major features. First, there is a near degeneracy of the $T=0$ and 1 states in the absence of the Coulomb interaction. Second, the particle unbound nature of these states produces large Coulomb mixing matrix elements. Their RCCSM calculation predicts an effective admixture amplitude of $|\beta| = 0.45$ which is in excess of the lower limit established by experiment, and predicts widths of 476 keV FWHM and 266 keV FWHM for the 19.25- and 19.65-MeV levels, respectively.

Figure 18 shows new π^+, π^-, and difference spectra at $\theta_{lab} = 70°$ for 180 MeV incident pion energy. Improved resolution (180 keV) and statistics permit an accurate determination for the widths and relative yields. The width for the 19.25-MeV level is estimated to be 390±30 keV FWHM, while that of the 19.65-MeV level is estimated to be 200±25 keV FWHM. The values for $\sigma_{\pi^+}/\sigma_{\pi^-}$ extracted from the spectra in Fig. 18 are 4.5±1.2 to 1 and 1 to 5.8±1.5 for the 19.25- and 19.65-MeV levels, respectively. The quoted errors include an estimated ±20% systematic fitting error applied to the π^+ yield of the 19.65-MeV level and to the π^- yield of the 19.25-MeV level. We have assumed that the resonant shapes for these states do not change from the π^+ to the π^- spectra. If the physical overlap of these resonances or any other 4^- structure is large, this assumption is not justified.

We have extracted values for the admixture amplitude by use of DWIA calculations and wave functions composed of separate isoscalar and isovector contributions. Independent estimates for β are thereby obtained from the $\sigma_{\pi^+}/\sigma_{\pi^-}$ ratios for each state, yielding $|\beta| = 0.58 \pm 0.05$ for the 19.25-MeV ratio and $|\beta| = 0.62 \pm 0.06$ for the 19.65-MeV ratio. Since these two estimates are in agreement, we conclude that the effective admixture amplitude, within the context of our model, is $|\beta| = 0.6 \pm 0.05$. The

TABLE II. Wave functions used in microscopic calculations.

E_x (MeV)	$[j_p j_h^{-1}]J$	α^a (fm^{-1})	$Z(T=0)^a$	$Z(T=1)^a$	$\Gamma_\lambda^{(\sigma)}$ (eV)
12.71	$[1p_{1/2}\,1p_{1/2}^{-1}]1$	0.513,[b] 0.625[c]	0.0445	−0.0028	0.35
	$[1p_{1/2}\,1p_{3/2}^{-1}]1$		−0.7317	0.0467	
	$[1p_{3/2}\,1p_{1/2}^{-1}]1$		−0.3611	0.0231	
	$[1p_{3/2}\,1p_{3/2}^{-1}]1$		−0.0142	0.0009	
15.11	$[1p_{1/2}\,1p_{1/2}^{-1}]1$	0.513,[b] 0.552[d]	0.0041	0.0636	37
	$[1p_{1/2}\,1p_{3/2}^{-1}]1$		0.0484	0.7578	
	$[1p_{3/2}\,1p_{1/2}^{-1}]1$		0.0239	0.3729	
	$[1p_{3/2}\,1p_{3/2}^{-1}]1$		0.0054	0.0840	
16.11	$[1p_{1/2}\,1p_{3/2}^{-1}]2$	0.610	0.0	−0.6796	0.67
	$[1p_{3/2}\,1p_{1/2}^{-1}]2$		0.0	0.1136	
	$[1p_{3/2}\,1p_{3/2}^{-1}]2$		0.0	−0.0607	
19.25	$[1d_{5/2}\,1p_{3/2}^{-1}]4$	0.620	0.4190	−0.3160	3.1×10^{-6}
19.65	$[1d_{5/2}\,1p_{3/2}^{-1}]4$	0.620	0.3160	0.4190	1.3×10^{-6}
4.44[e]	$[1d_{3/2}\,1s_{3/2}^{-1}]2$	0.575	0.079	0.0	11.3×10^{-3}
	$[1s_{1/2}\,1d_{3/2}^{-1}]2$		−0.0090	0.0	
	$[1d_{5/2}\,1s_{1/2}^{-1}]2$		−0.007	0.0	
	$[1s_{1/2}\,1d_{5/2}^{-1}]2$		−0.0097	0.0	
	$[1p_{3/2}\,1p_{1/2}^{-1}]2$		0.6201	0.0	
	$[1p_{1/2}\,1p_{3/2}^{-1}]2$		−0.8506	0.0	
	$[2p_{3/2}\,1p_{1/2}^{-1}]2$		0.0077	0.0	
	$[1p_{1/2}\,2p_{3/2}^{-1}]2$		−0.0188	0.0	
	$[1p_{3/2}\,1p_{3/2}^{-1}]2$		0.4471	0.0	
	$[2p_{1/2}\,1p_{3/2}^{-1}]2$		−0.0175	0.0	
	$[1p_{3/2}\,2p_{1/2}^{-1}]2$		0.0185	0.0	
	$[2p_{3/2}\,1p_{3/2}^{-1}]2$		0.0068	0.0	
	$[1p_{3/2}\,2p_{3/2}^{-1}]2$		0.0123	0.0	
	$[1d_{3/2}\,1d_{3/2}^{-1}]2$		0.0356	0.0	
	$[1d_{5/2}\,1d_{3/2}^{-1}]2$		0.0213	0.0	
	$[1d_{3/2}\,1d_{5/2}^{-1}]2$		−0.0271	0.0	
	$[1d_{5/2}\,1d_{5/2}^{-1}]2$		0.0646	0.0	
7.64	$[1p_{1/2}\,1p_{1/2}^{-1}]0$	0.380	0.6076	0.0	1.74 fm[2f]
	$[1p_{3/2}\,1p_{3/2}^{-1}]0$		0.183 28	0.0	
9.64[e]	$[1d_{5/2}\,1p_{1/2}^{-1}]3$	0.575	0.3686	0.0	0.22×10^{-3}

4^- doublet is apparently almost totally isospin mixed and more accurately described as a proton and a neutron state.

The particle-hole spectroscopic amplitudes for the isoscalar and isovector components of the 4^- spin transition densities were chosen such that $|\beta|=0.6$ and that the cross section at the peak of the 180-MeV π^+ angular distribution for the 19.25-MeV level is reproduced. We are free to choose the overall normalization for the 4^- transitions since the lower 4^- state has not been identified in electron scattering data.[57] The centroid of 19.59 MeV from Ref. 57 is near the upper 4^- state from the present work. The harmonic oscillator parameter for our calculations is the same as that used for the 4^- transitions in ^{16}O in Ref. 63 with the appropriate center-of-mass correction. Possible shape differences between proton and neutron radial wave functions as discussed by Siciliano and Weiss[68] are ignored. Table II contains the transition density parameters used for these calculations. The agreement at the maximum produced by our energy-shifted interaction is quite good over the entire energy range.

Next we consider the transitions to the 1^+ doublet at 12.71 and 15.11 MeV. Again, isospin mixing between the two levels results in π^+/π^- asymmetries.[71,72] The admixture amplitude for these states has been determined to be $|\beta|=0.06\pm0.01$ from fitting the $\sigma_{\pi^+}/\sigma_{\pi^-}$ ratios for the 100-, 116-, and 130-MeV 25° and 30° data.[6] Unlike the case for the 4^- states, there has been extensive study of this classic example of isospin mixing between analog states using both electromagnetic and hadronic probes.[73] Although estimates vary widely, the value determined from the pion data is in agreement with the back-angle electron-scattering results of Flanz *et al.*[73]

For the 1^+ calculations shown in Figs. 14 and 15, the isoscalar and isovector spin transition densities are given in terms of particle-hole spectroscopic strengths taken from the model of Cohen and Kurath[74] (CK) and perturbed by the admixture amplitude. The 15.11-MeV level was renormalized by 1.1 to produce the $M1$ strength as determined from fitting the isovector electron-scattering transverse form factor.[60] The validity of CK wave functions for ^{12}C is supported by electron-scattering results for the 15.11-MeV level[75] and proton stripping data.[76] (Electron scattering to the 12.71-MeV level is also well repro-

TABLE II. (*Continued*).

E_x (MeV)	$[j_p j_h^{-1}]J$	α[a] (fm^{-1})	$Z(T=0)$[a]	$Z(T=1)$[a]	$\Gamma_\chi^{(\sigma)}$ (eV)
	$[1p_{1/2}\ 1d_{5/2}^{-1}]3$		0.2037	0.0	
	$[1d_{3/2}\ 1p_{3/2}^{-1}]3$		−0.4201	0.0	
	$[1p_{3/2}\ 1d_{5/2}^{-1}]3$		−0.2192	0.0	
	$[1d_{5/2}\ 1p_{3/2}^{-1}]3$		0.6973	0.0	
	$[1p_{3/2}\ 1d_{5/2}^{-1}]3$		0.2037	0.0	
	$[1d_{5/2}\ 2p_{1/2}^{-1}]3$		0.0141	0.0	
	$[1d_{3/2}\ 2p_{3/2}^{-1}]3$		−0.0129	0.0	
	$[1d_{5/2}\ 2p_{3/2}^{-1}]3$		0.0202	0.0	
	$[2s_{1/2}\ 1f_{5/2}^{-1}]3$		0.0002	0.0	
18.25[e]	$[1d_{3/2}\ 1p_{1/2}^{-1}]2$	0.550	−0.0159	0.0616	0.243
	$[1p_{1/2}\ 1d_{3/2}^{-1}]2$		−0.0078	0.0030	
	$[1d_{5/2}\ 1p_{1/2}^{-1}]2$		0.0604	−0.0233	
	$[2s_{1/2}\ 1p_{3/2}^{-1}]2$		−0.1420	0.0550	
	$[1d_{3/2}\ 1p_{3/2}^{-1}]2$		0.0552	−0.0214	
	$[1d_{5/2}\ 1p_{3/2}^{-1}]2$		−0.3990	0.1540	
	$[1p_{3/2}\ 1d_{5/2}^{-1}]2$		−0.0414	0.0160	
	$[1d_{5/2}\ 2p_{3/2}^{-1}]2$		−0.0112	0.0434	
19.4[e]	$[1d_{3/2}\ 1p_{1/2}^{-1}]2$	0.550	0.0616	0.0159	0.652
	$[1p_{1/2}\ 1d_{3/2}^{-1}]2$		0.0030	0.0078	
	$[1d_{5/2}\ 1p_{1/2}^{-1}]2$		−0.0233	−0.0604	
	$[2s_{1/2}\ 1p_{3/2}^{-1}]2$		0.0550	0.1420	
	$[1d_{3/2}\ 1p_{3/2}^{-1}]2$		−0.0214	−0.0552	
	$[1d_{5/2}\ 1p_{3/2}^{-1}]2$		0.1540	0.3990	
	$[1p_{3/2}\ 1d_{5/2}^{-1}]2$		0.0160	0.0414	
	$[1d_{5/2}\ 2p_{3/2}^{-1}]2$		0.0434	0.0112	

[a]Values quoted for α, $(M\omega/\hbar)^{1/2}$, and the spectroscopic amplitudes are shell-model values. The standard c.m. correction is used in the calculation. Spectroscopic amplitudes have the convention that for a pure particle-hole excitation the value is unity.
[b]Harmonic oscillator parameter taken from Ref. 77.
[c]Harmonic oscillator parameter taken from Ref. 73.
[d]Harmonic oscillator parameter taken from Ref. 75.
[e]Glasgow wave functions.
[f]Value for reduced matrix element, $M_\chi^{(E)}$.

duced by CK wave functions if the above admixture amplitude is included.[73]) Results for two differing values for the harmonic oscillator parameter are shown in Figs. 14 and 15. In both cases the solid lines represent a value taken from Ref. 77 which gave reasonable results for proton scattering to the 15.11-MeV level. The dashed lines represent calculations using oscillator parameters taken from fits to electron-scattering data. For the 15.11-MeV level, we use the results of Dubach and Haxton,[75] who fitted both low- and high-q electron-scattering data. For the 12.71-MeV transition, the oscillator parameter is taken from the fit to the 12.71-MeV transverse form factor of Ref. 73. The particle-hole amplitudes and the oscillator parameters used in these calculations are given in Table II.

The results of both calculations give credible results over the full energy range for the 12.71-MeV level considering the quality of the data past the first maximum. The strength of the interaction is reasonably well reproduced by the p-wave form of the spin-orbit operator using the electron-scattering or proton-scattering results for the transverse spin transition density. The two oscillator parameters exhibit somewhat differing energy dependencies at the maximum, with that taken from electron scattering appearing preferable. However, we have omitted Fermi momentum corrections to the DWIA which can contribute to the 1^+ cross sections. The contribution coming from coupling to the nuclear convection currents through the non-spin-flip components of the interaction has been estimated in Ref. 78 for the 12.71-MeV transition using the correction term of Siciliano and Walker.[3] The effect of this Fermi momentum correction term is to increase the cross sections below the resonance, $\simeq$20% at 100 MeV, and to decrease the cross sections above the resonance, $\simeq$15% at 250 MeV. Therefore we cannot distinguish between the Fermi momentum corrections of Siciliano and Walker and the shape of the spin transition density by considering only the magnitude of the cross sections at the maximum.

The general agreement that we obtain for the isoscalar 1^+ transition is in sharp contrast to the results for the isovector transition to the 15.11-MeV level. The transverse

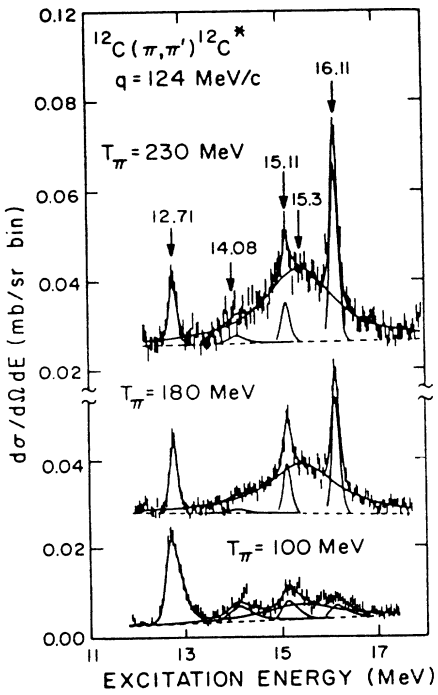

FIG. 19. Q-value spectra for π^+ inelastic scattering in the region of the 1^+ transitions in ^{12}C for incident pion energies of 100, 180, and 230 MeV at a constant q.

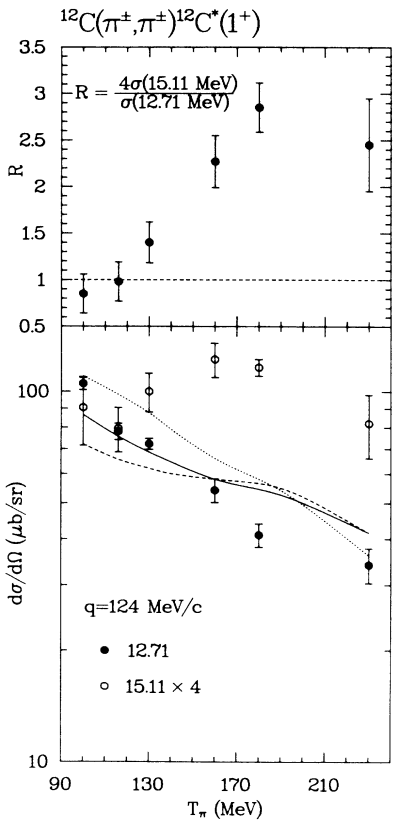

FIG. 20. Top: Ratio of the extrapolated cross sections for inelastic scattering to the isovector ($\times 4$) and isoscalar 1^+ states in ^{12}C at a constant q vs incident pion energy. Bottom: Comparison of extrapolated cross sections for scattering to the 12.71- and 15.11-MeV levels to DWIA calculations. The solid (dashed) curve are calculations for the 12.71-MeV (15.11-MeV) level. The dotted curve includes an estimation of the Fermi momentum correction for the 12.71-MeV transition.

spin transition density for the 15.11-MeV level is known to be well represented by CK wave functions from electron scattering.[60] The pion-scattering results for the 12.71-MeV level, which the CK wave functions give as a near relative to the 15.11-MeV level, support this assertion. However, the DWIA calculations for pion inelastic scattering to the 15.11-MeV level systematically underestimate the cross sections in the region of the resonance. Figure 19 demonstrates that the relative yield for the 1^+ levels can clearly be seen to change with energy in the Q-value spectra. Figure 20 compares the excitation functions for averaged π^+ and π^- data (averaged to remove Coulomb effects) near the first maximum, $q = 124$ MeV/c, for the 12.71 and 15.11-MeV levels. The data and calculations for the isovector transition have been multiplied by 4, the expected ratio for isoscalar and isovector transitions, assuming $\Delta_{3/2,3/2}$ dominance.[58] The solid (long dashed) curve is the DWIA prediction for averaged π^+ and π^- cross sections for the 12.71-MeV (15.11-MeV) transition. The dotted curve is a prediction for the 12.71-MeV transition including the Fermi momentum correction term. As was pointed out in Ref. 78, both the shape and magnitude of the 15.11-MeV excitation function are difficult to explain in terms of either uncertainties in spin transition densities or in any of the various pieces of the non-charge-exchange π-A interaction proposed or observed to date. It has been suggested that the structure in the 1^+ isovector transition be attributed to $\Delta_{3/2,3/2}$ particle-nucleon hole ($\Delta_{3/2,3/2}$-h) admixtures in the isovector state.[78] In this model the isospin of the $\Delta_{3/2,3/2}$, $T = \frac{3}{2}$, can couple with the isospin of the nucleon hole, $T = \frac{1}{2}$, to affect isovector but not isoscalar transitions. Although no detailed model for the π-$\Delta_{3/2,3/2}$ interaction is available, an estimate of the necessary admixture of $\Delta_{3/2,3/2}$-h component in the 15.11-MeV level was obtained by using the calculated contribution of the 1^+ $\Delta_{3/2,3/2}$-isobar hole state to the total π-A cross section in ^{12}C.[79] The $\Delta_{3/2,3/2}$-h admixture necessary to produce the observed enhancement for the 15.11-MeV state was found to be $|\beta| \geq 0.005$. This implies that pion-induced inelastic isovector transitions may be quite sensitive to even small admixtures of $\Delta_{3/2,3/2}$-h components in the wave functions. Similar enhancement of the $1^+ \rightarrow 0^+$ isovector transition in ^6Li has been observed.[80] Calculations for ^{12}C in a delta-hole model also predict this effect.[81]

We next consider the natural-parity, isovector transition to the 2^+ state at 16.11 MeV in ^{12}C. This state is predicted to have about equivalent matter and spin densities.[74] Figure 21 shows the relative radial dependences of the transitions used in these calculations. While there is gen-

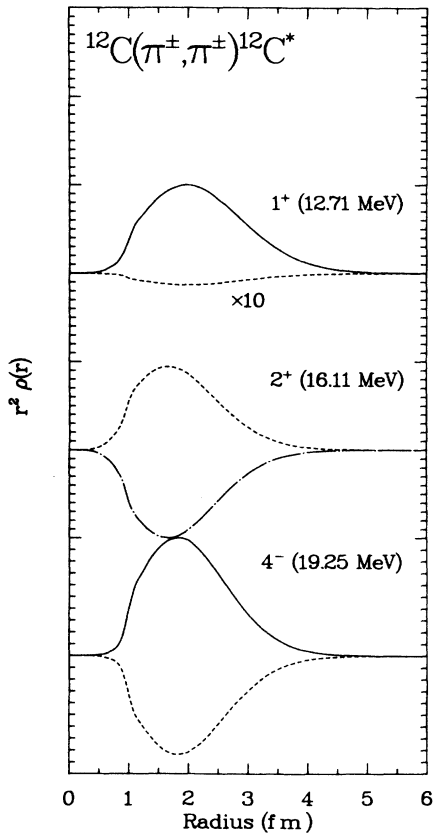

FIG. 21. Components of the radial transition densities for the isoscalar 1^+, the isovector 2^+, and the lower 4^- transition in ^{12}C. The solid curves represent the isoscalar spin-density component and the dashed curves represent the isovector spin-density. The dashed-dotted curve for the 2^+ represents the isovector matter density for this natural parity transition.

eral agreement that CK wave functions reproduce the shape of the inelastic electron-scattering longitudinal form factor, there is general disagreement as to the required normalization. Measurements for the electric transition width, $\Gamma_\lambda^{(E)}$, range from 0.35±0.04 (Ref. 82) to 0.75±0.16 eV,[72] whereas the CK prediction is 0.67 eV. The situation for the transverse spin density is somewhat less confusing. The CK prediction without renormalization gives rough agreement with the measured electron-scattering transverse form factor.[59] For these calculations we use the CK wave functions without renormalization of either the matter or the spin density and take the harmonic oscillator parameter from the electron-scattering results. Figure 16 (solid curves) shows the results for the particle-hole spectroscopic amplitudes given in Table II. The dashed curves show results considering the matter density alone. It is interesting to note that the effect of the large spin density is to increase the forward-angle cross sections at lower energies while increasing the back-angle cross sections at the higher energies. Although the CK wave functions appear to produce approximately the correct strengths at both the higher and lower energies, there is a systematic underestimation of the cross sections near resonance.

Figure 22 compares extrapolated values of the measured cross sections for the isovector 2^+ transition near the maximum, $q = 150$ MeV/c, to the DWIA predictions. For this natural-parity transition, possible $\Delta_{3/2,3/2}$-h admixtures (or Fermi momentum corrections to the DWIA for that matter) could be seen as an interference in either or both the spin-dependent or the spin-independent components of the pion-nucleus interaction. Additionally, the $M1$ transition decay widths[19] of the 12.71- and 4.44-Mev levels indicate that coupled-channel effects may be significant. We are thus discouraged from asserting that the enhancement observed in the excitation function for the 16.11-MeV level can be construed as evidence for $\Delta_{3/2,3/2}$-h components in the nuclear wave functions. We do note, however, that the structure in the excitation function for pion-induced inelastic scattering to the 2^+ level at 16.11 MeV is similar to that observed for the isovector 1^+ level in both magnitude and shape.

Finally, we consider states at 18.25±0.03 (with a width of 230±20 keV FWHM), 18.6±0.05 (with a width of 250±50 keV FWHM), and 19.4 MeV (with a width of 350±50 keV FWHM) which we identify as 2^- levels. The combined structure near 18.5 MeV, which is seen in both electron scattering[57,83] and proton scattering[84] and thought to be 2^-, is resolved into two levels by compar-

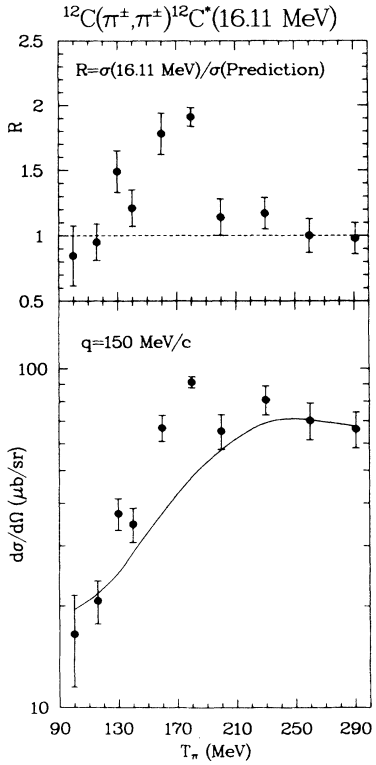

FIG. 22. Top: Ratio of the extrapolated cross sections for inelastic scattering to the isovector 2^+ state in ^{12}C at a constant q to absolute DWIA predictions vs incident pion energy. Bottom: Comparison of extrapolated cross sections for scattering to the 16.11-MeV level to DWIA calculations.

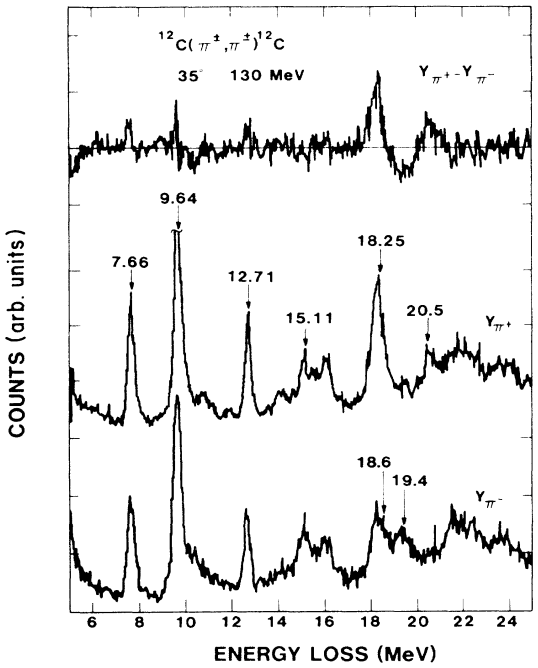

FIG. 23. Q-value spectra for π^+, π^-, and their difference for inelastic scattering at $T_\pi = 130$ MeV and $\theta_{lab} = 35°$.

ison of π^+ and π^- spectra. Owing to the overlap and possible interference of the two lower levels, there is considerable ambiguity in the determination of line shapes and we estimate the overall systematic uncertainty to be ±25%. Figures 23 and 24 show π^+, π^-, and the $\pi^+ - \pi^-$ difference spectra at 130 and 180 MeV. At both

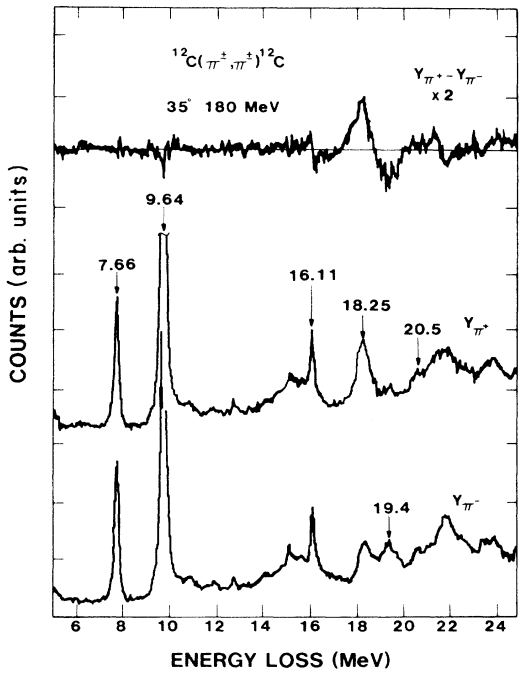

FIG. 24. Same as Fig. 23, except $T_\pi = 180$ MeV.

energies isospin mixing between the 18.25-MeV level and a state at 19.4 MeV is evident with a hint of further asymmetry at 20–21 MeV. The 18.25- and 18.6-MeV levels do not appear to be isospin mixed, as the extracted cross section for the 18.6-MeV level is about 65 μb/sr at the maximum for both π^+ and π^-. Since 2^- strength near 19.4 MeV has been observed in both electron scattering,[57,83,85] and proton scattering,[84] the assignment of 2^- remains consistent. Figure 25 compares the measured cross sections for the 18.25 MeV level to calculations assuming a dominantly isoscalar 2^- transition with an admixture amplitude of 0.36 for the isovector component. Table II gives the spectroscopic amplitudes used for these calculations. Our choice of amplitudes is somewhat arbitrary as renormalization of single particle excitation of $[1d_{5/2}\text{-}1p_{3/2}^{-1}]2^-$ gives essentially the same results. The spectroscopic amplitudes quoted are the results of renormalization, by a factor of 0.7, of the dominant components from Glasgow calculations[86] for a 2^-, $T=0$ state

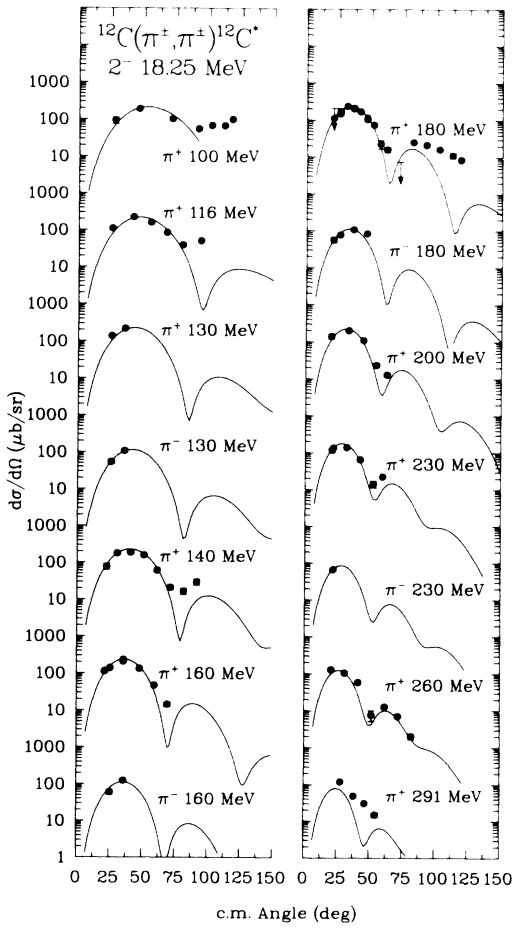

FIG. 25. Differential cross sections for pion-induced inelastic scattering to the 18.25-MeV level in ^{12}C in the region 100–300 MeV incident pion energy. The curves are the results of microscopic calculations using the particle-hole spectroscopic amplitudes given in Table II.

predicted to be near 18 MeV in excitation. The harmonic oscillator parameter was chosen to reproduce approximately the position of the first minimum. With the exception of the 291 MeV data, the agreement is quite convincing.

Figure 26 compares the cross sections for the 19.4-MeV level with calculations assuming that this is the upper member of an isospin-mixed 2^- doublet. Although the π^- results are consistent with this assumption, calculations for π^+ greatly underestimate the observed cross sections at all energies. Provided that the extraction of cross sections of π^+ scattering to the 19.4 MeV level is accurate, simple two-state mixing between the 18.25- and 19.4-MeV levels must be ruled out. This suggests further mixing with at least one other broad 2^- state, possibly in the region of 23–26 MeV in excitation.[87]

In addition to the 2^- states mentioned above, the 2^- state at 11.83 MeV is weakly excited in pion scattering. The differential cross section at 180 MeV and 35° is about 20 μb/sr. The 2^- state at 16.6 MeV (Ref. 60) was not observed. The observation of additional 2^- structure in the region 18–19 MeV and the observation of isospin mixing should assist in clarification of the 2^- structure in ^{12}C.

It is interesting to note that DWIA calculations for the collective 2^+, 0^+, and 3^- transitions which gave reasonable agreement at resonance energies and above fail badly at the lowest energies. On the other hand, microscopic DWIA calculations for the 1^+ and 4^- doublets and the isovector 2^+ transitions are reasonably well reproduced at these energies. Microscopic calculations normalized to $B(C\lambda)\downarrow$ have been performed for the collective 2^+ and 3^- transitions including the full $2\hbar\omega$ basis for the natural-parity components and the $1\hbar\omega$ basis for the unnatural-parity components using Glasgow wave functions,[86] which are represented by the dashed-dotted curves in Figs. 7–10. CK wave functions were used for the 0^+ transition. These calculations, which now include both spin-independent and spin-dependent components and contributions from outside the p shell, do little to resolve the difficulty at the lower energies. Comparison of the radial transition densities, Figs. 12 and 21, and the sensitivity function, Fig. 13, does not suggest that the discrepancy at low energies is associated with the particular region of the nuclear medium being sampled by the transition or with a failure to predict the effect of the distortions as the pion penetrates the nuclear surface. The success for the 4^- transitions over the full energy range would also suggest that, to first order, kinematics for the inelastic pion-nucleus interaction are being adequately treated.

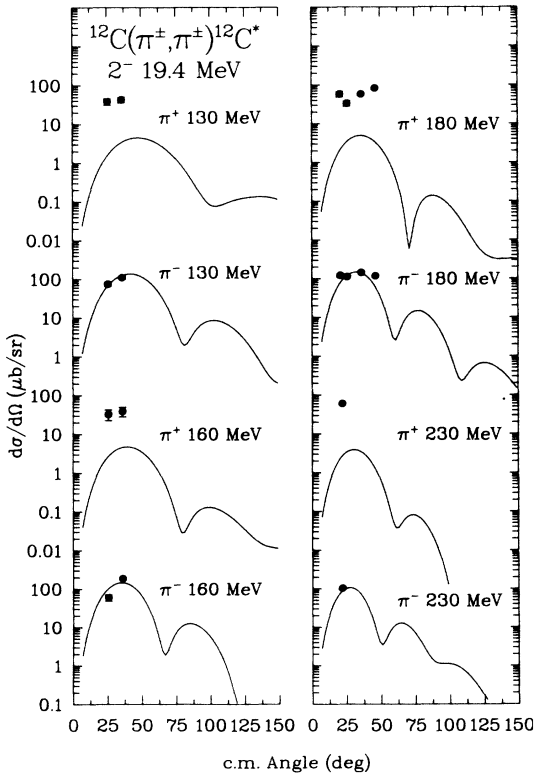

FIG. 26. Same as Fig. 25, except for the 19.4-MeV level.

VI. CONCLUSIONS

From these results for ^{12}C we conclude that pion-induced inelastic scattering in the forward hemisphere can be explained over the entire energy range of the $\Delta_{3/2,3/2}$ by simple zero-range, frozen-target DWIA calculations for certain classes of transitions. Strongly excited transitions involving only the spin-dependent component of the π-A interaction exhibit energy dependences which agree well with those of these calculations. The results for the 4^- transitions indicate that some correction to the frozen-target approximation to account for the Fermi motion of the target nucleons is necessary, at least for transitions involving the spin-dependent component of the π-A interaction, which has a rapidly changing energy dependence. The energy dependence for the transition to the 2^- state at 18.25 MeV is also well reproduced by our calculations. For the isoscalar 1^+ transition, where presumably the strength is known, we obtain semiquantitative agreement between data and absolute calculations. However, the quality of these data preclude investigation of subtle effects such as the influence of nuclear-current and spin-current densities. Likewise, transitions to the collective 2^+, 0^+, and 3^- states are reasonably reproduced for incident pion energies above 140 MeV using empirically determined transition densities.

On the other hand, the transitions to the isovector 1^+ level at incident pion energies near 180 MeV are grossly underestimated by our calculations. This enhancement may be an indication of the sensitivity of pion-induced inelastic scattering to delta particle–nucleon hole components in the nuclear wave function. Cross sections which are in excess of the calculated values have also been observed for the isovector transition to the 16.11-MeV level. Although the magnitude and shape are similar to the structure which has been observed for the isovector 1^+ state, the structure for the 2^+ level may be due to an inadequate description of the transition. We have also observed enhancements of backward angle cross sections at low energies for the 4.44-, 7.66-, and 9.64-MeV levels which are not predicted in our model. These enhancements are not observed in the transitions above 10 MeV in excitation, where the calculated values agree with the

low energy data. In particular, it can be seen that the 100-MeV angular distributions for the 2^+ state at 4.44 MeV and for the 2^+ state at 16.11 MeV have different shapes.

In the course of this work, we have identified new features in the structure of ^{12}C. The admixture amplitude for isospin mixing and the spectroscopic strengths for the 4^- doublet near 19.25 MeV have been estimated. The observation of isospin mixing between levels at 18.25 and 19.4 MeV and the shape of the angular distributions confirm an assignment of 2^- for these levels. We have also observed additional fragmentation of the 2^- structure in the region 18–19 MeV.

ACKNOWLEDGMENTS

We would like to thank J. A. Carr and F. Petrovich for providing us with a copy of their inelastic scattering potential code and also for their helpful discussions. We would also like to thank W. C. Haxton for furnishing Glasgow wave functions for the 2^+ and 3^- states. This work was supported in part by the U.S. Department of Energy and the Robert A. Welch Foundation.

---

*Present address: Los Alamos National Laboratory, Los Alamos, NM 87545.

†Present address: The University of New Mexico, Albuquerque, NM 87131.

‡Present address: The University of British Columbia, Vancouver, British Columbia, Canada V6T 2A3.

§Present address: 2072 Saint Blaise, Chair D'ane, Switzerland.

[1]C. F. Moore *et al.*, Phys. Lett. **80B**, 38 (1978).

[2]W. B. Cottingame *et al.*, Bull. Am. Phys. Soc. **24**, 821 (1979).

[3]E. R. Siciliano and G. E. Walker, Phys. Rev. C **23**, 2661 (1981).

[4]W. B. Cottingame *et al.*, in *Proceedings of the IInd International Topical Conference on Meson-Nuclear Physics, Houston, Texas, 1979,* edited by E. Hungerford (AIP, New York, 1979), p. 272.

[5]C. L. Morris *et al.*, Phys. Lett. **86B**, 31 (1979).

[6]C. L. Morris *et al.*, Phys. Lett. **99B**, 387 (1981).

[7]See AIP Document No. PRVCA-36-230-39 for 39 pages of tabulated cross sections and for the appendices deriving the energy shift for the elastic and inelastic scattering. Order by PAPS number and journal reference from American Institute of Physics, Physics Auxiliary Publication Service, 335 E. 45 St., New York, NY 10017. The price is $1.50 for microfiche, or $6.35 for photocopies. Airmail additional. Make check payable to American Institute of Physics. This material appears in the monthly *Current Physics Microfilm* edition of all journals published by AIP, on the frames following this article.

[8]R. J. Peterson *et al.*, Nucl. Instrum. Methods **129**, 47 (1975).

[9]H. A. Thiessen *et al.*, Los Alamos Scientific Report LA-6663-MS, 1977.

[10]C. L. Morris, H. A. Thiessen, and G. W. Hoffmann, IEEE Trans. Nucl. Sci. **NS-25**, 141 (1978).

[11]L. G. Atencio, J. F. Amann, R. L. Boudrie, and C. L. Morris, Nucl. Instrum. Methods **187**, 381 (1981).

[12]C. L. Morris, Nucl. Instrum. Methods **196**, 263 (1982).

[13]M. J. Devereux, Los Alamos Scientific Laboratory Report LA-7851-T, 1979.

[14]J. F. Amann *et al.*, IEEE Trans. Nucl. Sci. **NS-26**, 4389 (1979).

[15]R. L. Boudrie *et al.*, IEEE Trans. Nucl. Sci. **NS-26**, (1979).

[16]D. Dodder, private communication.

[17]P. J. Bussey *et al.*, Nucl. Phys. **B58**, 363 (1973).

[18]L. E. Smith (unpublished).

[19]F. Ajzenberg-Selove, Nucl. Phys. **A433**, 1 (1985).

[20]D. J. Ernst and G. Miller, Phys. Rev. C **21**, 1472 (1980).

[21]L. C. Liu and C. M. Shakin, in *Progress in Particle and Nuclear Physics,* edited by D. Wilkinson (Pergamon, New York, 1980), Vol. 5, p. 207.

[22]A. W. Thomas and R. H. Landau, Phys. Rep. **58**, 121 (1980).

[23]M. Johnson and D. Johnson, Phys. Rev. C **20**, 1064 (1980).

[24]L. S. Kisslinger, Phys. Rev. **98**, 761 (1955).

[25]E. R. Siciliano and G. E. Walker, Phys. Rev. C **13**, 257 (1976).

[26]D. J. Ernst and M. B. Johnson, Phys. Rev. C **17**, 247 (1978).

[27]D. Ernst and M. Johnson, Phys. Rev. C **22**, 651 (1980).

[28]J. T. Londergan, K. M. McVoy, and E. J. Moniz, Ann. Phys. (N.Y.) **86**, 147 (1974).

[29]J. Piffaretti *et al.*, Phys. Lett. **67B**, 289 (1977); **71B**, 324 (1978).

[30]W. B. Cottingame and D. B. Holtkamp, Phys. Rev. Lett. **45**, 1828 (1980).

[31]R. A. Eisenstein and G. A. Miller, Comput. Phys. Commun. **8**, 130 (1974), and private communication.

[32]E. H. Auerbach, D. M. Fleming, and M. M. Sternheim, Phys. Rev. **162**, 1683 (1967).

[33]G. Rowe, M. Salomon, and R. H. Landau, Phys. Rev. C **18**, 384 (1978).

[34]C. W. DeJager, H. DeVries, and C. DeVries, At. Data Nucl. Data Tables **14**, 479 (1974).

[35]I. Sick and J. S. McCarthy, Nucl. Phys. **A150**, 631 (1970).

[36]I. Sick, Nucl. Phys. **A218**, 509 (1974).

[37]J. P. Albanese *et al.*, Nucl. Phys. **A350**, 301 (1980).

[38]K. S. Dhuga *et al.*, Phys. Rev. C **32**, 2208 (1985).

[39]R. A. Bryan, C. A. Dominguez, and B. J. Ver West, Phys. Rev. C **22**, 160 (1980).

[40]C. A. Dominguez and B. J. Ver West, Phys. Lett. **89B**, 333 (1980).

[41]J. W. Durso, A. D. Jackson, and B. J. Ver West, Nucl. Phys. **A282**, 404 (1977).

[42]B. J. Ver West, Phys. Lett. **83B**, 161 (1979).

[43]Nen-Chinh Wei and M. K. Banerjee, Phys. Rev. C **22**, 2052 (1980).

[44]D. J. Ernst, private communication.

[45]H. Crannell and T. Griffy, Phys. Rev. **136**, B1580 (1964).

[46]H. Crannell, Phys. Rev. **148**, 1107 (1966).

[47]F. Binon *et al.*, Nucl. Phys. **B17**, 168 (1970).

[48]C. L. Morris *et al.*, Phys. Rev. C **24**, 231 (1981).

[49]K. G. Boyer, W. B. Cottingame, and D. B. Holtkamp, distorted wave code UTDWPI (unpublished), adapted from the code DWPI by R. A. Eisenstein and G. A. Miller, Comput. Phys. Commun. **11**, 95 (1976).

[50]R. A. Eisenstein and G. A. Miller, Comput. Phys. Commun. **11**, 95 (1976).

[51]L. J. Tassie, Aust. J. Phys. **9**, 407 (1956).

[52]P. Strehl, Z. Phys. **234**, 418 (1970).

[53]A. Nakata, Y. Torizuka, and Y. Horikawa, Phys. Rev. Lett. **27**, 745 (1971).

[54]C. Gustaffsson and E. Lambert, Ann. Phys. (N.Y.) **111**, 304 (1978).
[55]K. W. Jones *et al.*, Phys. Rev. C **33**, 17 (1986).
[56]D. A. Sparrow and W. J. Gerace, Phys. Rev. Lett. **41**, 1101 (1978).
[57]R. S. Hicks *et al.*, Phys. Rev. C **30**, 1 (1984).
[58]M. K. Gupta and G. E. Walker, Nucl. Phys. **A256**, 444 (1976).
[59]J. B. Flanz *et al.*, Phys. Rev. Lett. **41**, 1642 (1978).
[60]U. Deutschmann, G. Lahm, R. Neuhausen, and J. C. Bergstrom, Nucl. Phys. **A411**, 337 (1983).
[61]M. Buenerd, P. Martin, P. DeSaintignon, and J. M. Loiseaux, Nucl. Phys. **A286**, 377 (1977).
[62]R. J. Peterson *et al.*, Phys. Rev. C **21**, 1030 (1980).
[63]J. A. Carr, F. Petrovich, D. Halderson, D. B. Holtkamp, and W. B. Cottingame, Phys. Rev. C **27**, 1636 (1983).
[64]K. Stricker, H. McManus, and J. A. Carr, Phys. Rev. C **19**, 929 (1979).
[65]J. A. Carr, private communication.
[66]E. R. Siciliano, invited talk given at LAMPF Workshop on Pion Single Charge Exchange, Los Alamos Scientific Laboratory Report LA-7892-6, 1979.
[67]T. Suzuki, S. Krewald, and J. Speth, Phys. Lett. **107B**, 9 (1981).
[68]E. R. Siciliano and D. L. Weiss, Phys. Lett. **93B**, 371 (1980).
[69]D. Halderson, R. J. Philpott, J. A. Carr, and F. Petrovich, Phys. Rev. C **24**, 1095 (1981).
[70]D. Halderson and R. J. Philpott, Nucl. Phys. **A345**, 141 (1980), and references contained therein.
[71]A. Yamaguchi, T. Terasawa, K. Nakahara, and Y. Torizuka, Phys. Rev. C **3**, 1750 (1971).
[72]A review of the subject can be found in E. G. Adelberger, R. C. Marrs, K. A. Snover and J. Bussoletti, Phys. Rev. C **15**, 484 (1977).
[73]J. B. Flanz *et al.*, Phys. Rev. Lett. **43**, 1922 (1979).
[74]S. Cohen and D. Kurath, Nucl. Phys. **73**, 1 (1965), as quoted in T. S. Lee and D. Kurath, Phys. Rev. C **21**, 293 (1980).
[75]J. Dubach and W. C. Haxton, Phys. Rev. Lett. **41**, 1435 (1978).
[76]P. B. Foot *et al.*, Phys. Rev. C **31**, 1133 (1985).
[77]J. R. Comfort *et al.*, Phys. Rev. C **21**, 2147 (1980).
[78]C. L. Morris *et al.*, Phys. Lett. **108B**, 172 (1982).
[79]K. Klingenbeck, M. Dillig, and M. G. Huber, Phys. Rev. Lett. **41**, 387 (1978).
[80]R. R. Kiziah *et al.*, Phys. Rev. C **30**, 1643 (1984).
[81]H. Hirata, F. Lenz, and M. Thies, Phys. Rev. C **28**, 785 (1983).
[82]A. Friebel *et al.*, Nucl. Phys. **A294**, 129 (1978).
[83]P. Antony-Spies, P. P. Delsanto, E. Spamer, A. Goldmann, and O. Titze, Phys. Lett. **31B**, 632 (1970).
[84]K. W. Jones *et al.*, Phys. Lett. **128B**, 281 (1983).
[85]H. Crannell and H. A. Dahl, Phys. Rev. **115**, 1062 (1967).
[86]J. Dubach and W. C. Haxton, private communication; wave functions were derived from the Los Alamos version (unpublished) of Glasgow computer code (unpublished) by R. R. Whitehead.
[87]C. F. Moore *et al.*, Phys. Rev. C **26**, 2561 (1981).
[88]T. W. Chen, Phys. Rev. C **13**, 1974 (1976); D. W. Hoock, Jr., Ph.D. thesis, New Mexico State University, 1978.
[89]J. A. Carr, private communication.
[90]Y. Horikawa, M. Thies, and F. Lenz, Nucl. Phys. **A345**, 386 (1980).
[91]H. A. Thiessen, private communiation.
[92]J. A. Jansen, R. Th. Peerdeman, and C. DeVries, Nucl. Phys. **A188**, 337 (1972).